nature communications

Article

https://doi.org/10.1038/s41467-026-76325-6

Heat stress promotes pre-tRNA capping to modulate cap-dependent translation in *Saccharomyces cerevisiae*

Received: 4 July 2025

Accepted: 27 July 2026

Published online: 07 August 2026

Check for updates

Ittoku Kikuchi[1], Takayuki Ohira[1] ✉, Taichi Nakatsuka[1], Yuma Ishigami[1,2] & Tsutomu Suzuki[1] ✉

Methylguanosine capping, a post-transcriptional modification of the 5′ terminus of RNA polymerase II transcripts, influences RNA function, stability, and protein synthesis. Previously, we identified the cap modification in specific transfer RNA (tRNA) precursors (pre-tRNAs) transcribed by RNA polymerase III in *Saccharomyces cerevisiae*, and demonstrated that pre-tRNA capping prevents 5′ exonucleolytic degradation of pre-tRNAs. Herein, we comprehensively mapped pre-tRNA capping and found that nearly all pre-tRNAs undergo cap modification. This analysis enabled precise determination of transcription start sites for all tRNA genes, and the capping efficiency was strongly influenced by the base-pairing probability between 5′ leaders and 3′ trailers of pre-tRNAs. Furthermore, pre-tRNA capping was significantly upregulated under heat stress, resulting in capped pre-tRNA-derived fragments. Capped pre-tRNAs modulated cap-dependent translation by sequestering eukaryotic initiation factor 4E (eIF4E). Overall, these findings suggest that pre-tRNA capping contributes to the regulation of cap-dependent translation under heat stress conditions in *Saccharomyces cerevisiae*.

Transfer RNA (tRNA) serves as an adapter molecule that links codons on mRNAs to their corresponding amino acids during protein synthesis[1,2]. In rapidly proliferating cells, a sufficient number of tRNAs must be continuously produced to maintain efficient protein synthesis. Recent studies revealed that appropriate regulation of tRNA abundance and its modification status contributes to mRNA stability[3,4] and correct folding of nascent proteins by maintaining an optimal speed for protein synthesis[5–7]. Dysregulation of tRNA abundance impairs global translation and healthy proteostasis, leading to pathological consequences[2,8].

tRNA quantity and functionality are dynamically regulated at various stages from birth to death, including transcription, processing, tRNA modification, intracellular localization, aminoacylation, decoding on the ribosome, and degradation[1,2,9]. Under combined heat stress and carbon source limitation, tRNA processing is inhibited, leading to accumulation of pre-tRNAs retaining their 5′ leader and 3′ trailer sequences[10]. Under normal growth conditions, ~50% of nascent transcripts, including pre-tRNAs, are continuously degraded[11,12]. However, during heat stress, unstable mature tRNAs and their precursors with hypomodification or structural abnormalities are rapidly degraded by surveillance systems[13,14]. Therefore, biogenesis and stability of tRNAs form a crucial layer of regulatory gene expression and are dynamically adjusted in response to changes in the cellular environment.

Transcription and biogenesis of cytoplasmic tRNAs have been extensively studied in *Saccharomyces cerevisiae*[1]. In total, 275 tRNA genes are encoded in the *S. cerevisiae* genome, giving rise to 42 distinct cytoplasmic tRNAs. Among them, 61 tRNA genes corresponding to 10 tRNA species contain introns in their anticodon loop[15].

Every tRNA gene contains internal promoters, known as A and B boxes, that are recognized by the transcription factor TFIIIC[16,17]. TFIIIB is recruited to an AT-rich sequence upstream of the transcription start site (TSS) of the tRNA gene, facilitating the recruitment of RNA

[1]Department of Chemistry and Biotechnology, Graduate School of Engineering, University of Tokyo, Bunkyo-ku, Tokyo, Japan. [2]Cold Spring Harbor Laboratory, Cold Spring Harbor, NY, USA. ✉e-mail: ohira_t@chembio.t.u-tokyo.ac.jp; ts@chembio.t.u-tokyo.ac.jp

https://doi.org/10.1038/s41467-026-76325-6

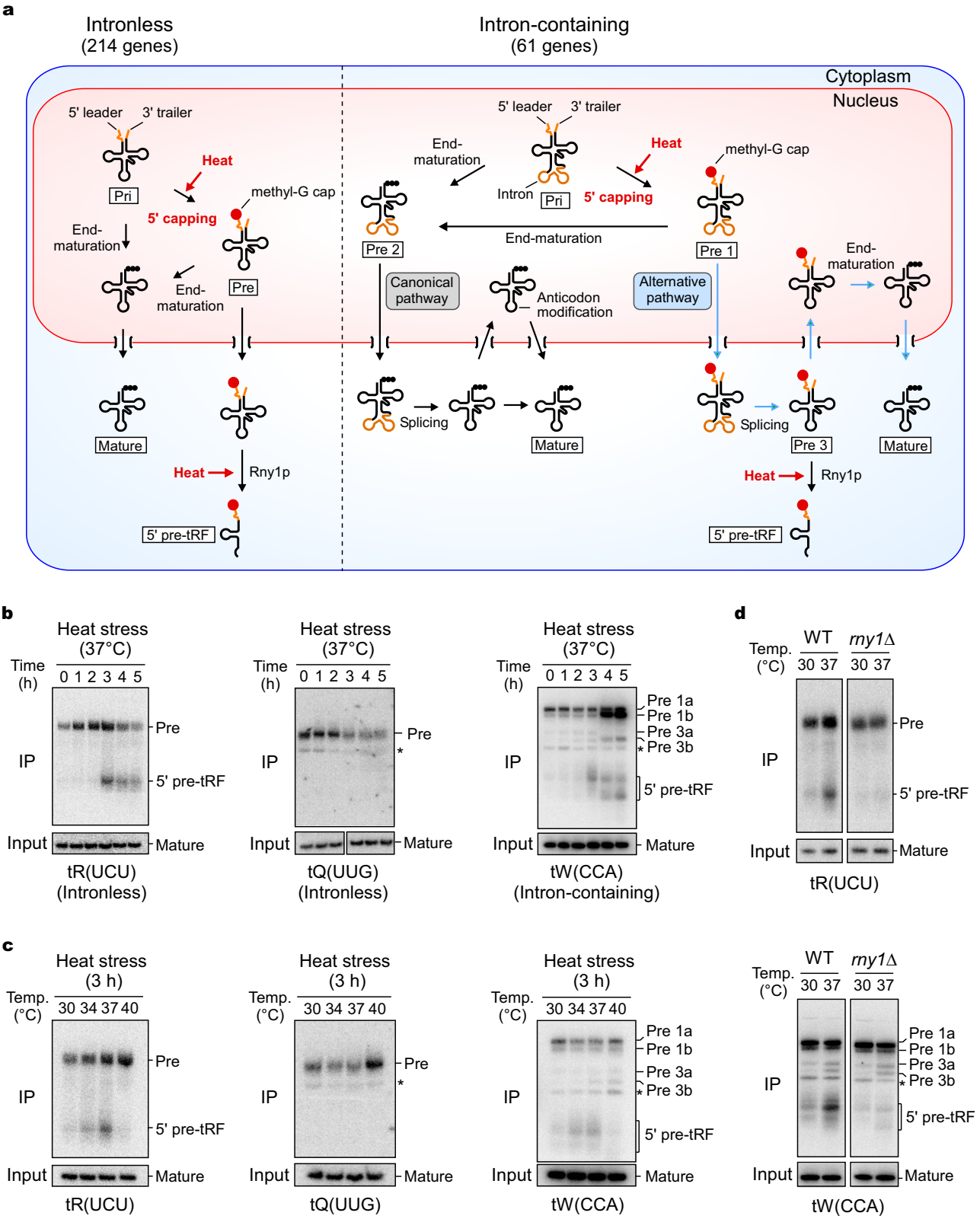

polymerase III (RNAPIII)[16,17]. TSSs of tRNA genes have been predicted in the *S. cerevisiae* genome, and some have been experimentally determined[17–19]. By contrast, transcription termination sites (TTSs) have been experimentally determined[17].

tRNA biogenesis begins in the nucleolus, where tRNA genes are transcribed by RNAPIII, producing primary tRNA transcripts (pri-tRNAs) that contain 5′ leader and 3′ trailer sequences, and in some cases, an intron in the anticodon loop[1] (Fig. 1a). Pri-tRNAs without introns undergo processing by RNase P and Trz1p to remove their 5′ leader and 3′ trailer sequences, respectively[20,21]. The 3′ trailer processing is further assisted by RNA binding proteins, La protein (Lhp1p) and Lsm2-8 complex, and several exonucleases[21,22]. Subsequently, Cca1p

Fig. 1 | Schematic diagram of tRNA maturation in *S. cerevisiae* and accumulation of capped pre-tRNAs and 5′ pre-tRNA fragments (pre-tRFs) under heat stress. a Schematic overview of tRNA maturation in *S. cerevisiae*. tRNA genes are transcribed by RNAPIII in the nucleus to produce primary transcripts (Pri) containing a 5′ leader, a 3′ trailer, and, in some cases, an intron. For intronless tRNAs (left), pri-tRNAs are processed into pre-tRNAs with immature ends (Pre) or into end-matured forms in the nucleus before being exported to the cytoplasm. RNA modifications are introduced throughout the maturation process. For intron-containing tRNAs (right), two maturation pathways exist. In the canonical pathway (black arrows), end-maturation occurs first (generating Pre 2), followed by splicing. In the alternative pathway (light blue arrows), pre-tRNAs with immature ends (Pre 1) are exported to the cytoplasm and spliced to generate Pre 3, which are re-imported into the nucleus for end-maturation. Some spliced pre-tRNAs are also imported back into the nucleus for additional modification. A 5′ cap structure (red circles) is post-transcriptionally added by the nuclear capping machinery. Heat stress induces 5′ capping and Rny1p-mediated cleavage of pre-tRNAs, generating 5′ pre-tRNA fragments (pre-tRFs) (red arrows). **b**,**c** Northern blotting and immunoprecipitation (IP)-Northern blotting of tRNAs. Total RNA from WT cells treated with or without heat stress at 37 °C for 0–5 h (**b**) or at 30–40 °C for 3 h (**c**) was analyzed by northern blotting (Input, lower panels) or IP using anti-cap antibodies followed by northern blotting (IP, upper panels). Probes were specific to tR(UCU), tQ(UUG), and tW(CCA). **d** Total RNA from WT and *rny1Δ* strains cultured with or without heat stress at 37 °C for 3 h was subjected to northern blotting and IP-northern blotting using probes for tR(UCU) and tW(CCA). tRNA precursors (Pre, Pre 1a/b, and Pre 3a/b), mature tRNAs (Mature), and 5′ pre-tRFs are indicated. The experiments were independently repeated three times with similar results. An asterisk (*) denotes a contaminating mature tRNA species. Source data are provided as a Source Data file.

adds the CCA sequence to the 3′ end, yielding a tRNA precursor (pre-tRNA) with mature ends (termed Pre)[23]. In the case of $tRNA^{His}$, one guanosine is added to the 5′ end by Thg1p[24]. Most RNA modifications are introduced during processing steps in the nucleus[1]. Pre-tRNAs are then exported to the cytoplasm through multiple nuclear export pathways mediated by Los1p, Crm1p, and Mex67-Mtr2[25]. Finally, pre-tRNAs undergo additional modifications by cytoplasmic tRNA-modifying enzymes, yielding fully-modified mature tRNAs[26].

Pri-tRNAs containing introns undergo processing and maturation through two distinct pathways (Fig. 1a)[19]. In the canonical pathway, pri-tRNAs are processed in the nucleus, similar to intronless tRNAs, yielding species with mature 5′ and 3′ ends (termed Pre 2). Pre 2 species are then exported to the cytoplasm, where introns are removed by tRNA splicing machinery on the mitochondrial outer membrane[27,28]. After splicing, intron-free pre-tRNAs are imported back into the nucleus, where modifications occur in the anticodon region, before being exported again to the cytoplasm[26].

By contrast, in the alternative pathway, tRNA splicing precedes end-maturation (Fig. 1a). Pre-tRNAs with immature ends (termed Pre 1) are exported to the cytoplasm via the Mex67-Mtr2 pathway[25], where they undergo splicing on the mitochondrial outer membrane, producing an intron-free form (termed Pre 3)[29]. Pre 3 species are then imported back into the nucleus[30], where their ends are processed before being re-exported to the cytoplasm. Thus, pre-tRNAs shuttle between the nucleus and cytoplasm, undergoing processing, splicing, and modification before achieving full maturation (Fig. 1a). Recent studies demonstrated that free introns of tRNAs (fitRNAs) induce degradation of mRNAs with complementary sequences, thereby regulating mRNA abundance under both basal and stress conditions[31].

tRNA fragments (tRFs) play important regulatory roles in various cellular processes[32,33]. Recent studies revealed that tRFs interact with ribosomes and translation initiation factors such as eukaryotic initiation factor 4 G (eIF4G), thereby regulating translation by suppressing protein synthesis under stress conditions[34]. Additionally, some tRFs bind to Argonaute proteins and perform a microRNA-like function to regulate mRNA stability and translation[35]. Beyond translation regulation, tRFs also participate in epigenetic control by influencing gene expression at the chromatin level[36]. In cancer, specific tRFs are involved in both tumor suppression and progression by either promoting or inhibiting cell proliferation and metastasis[37]. Recent research has also suggested that tRFs are secreted via extracellular vesicles and mediate intercellular communication in the tumor microenvironment and other physiological contexts[38].

The methylguanosine (methyl-G) cap is a highly conserved and essential RNA modification in eukaryotes. The N^7-methylguanosine (m^7G) cap is specifically added to the 5′ end of messenger RNA (mRNA) through a series of enzymatic reactions that occur co-transcriptionally on the C-terminal domain (CTD) of RNAPII[39–41] (Supplementary Fig. 1). Other RNAPII transcripts, including small nuclear RNAs (snRNAs) and small nucleolar RNAs (snoRNAs), undergo further methylation of the m^7G cap to form the $N^{2,2,7}$-trimethylguanosine (TMG) cap (Supplementary Fig. 1)[42]. These cap modifications play crucial roles in determining mRNA metabolism and function, including protection against 5′-exonucleolytic degradation, promotion of pre-mRNA splicing, nuclear export, and translation initiation by serving as recognition sites for cap-binding proteins[43,44]. Additionally, cap modifications are essential for distinguishing self from non-self RNA via RNA sensors in the innate immune system[44,45].

We previously discovered that 5′ cap modification occurs in a subset of pre-tRNAs in *S. cerevisiae* and human cells[19]. We termed this phenomenon “pre-tRNA capping”. This was an unexpected finding because tRNAs are RNAPIII transcripts. We also showed that the canonical capping enzyme Ceg1p is involved in pre-tRNA capping. Because RNAPIII lacks a CTD, pre-tRNA capping is likely introduced post-transcriptionally. Furthermore, we demonstrated that the cap structure on pre-tRNAs plays a role in preventing their degradation from the 5′ end.

In the present study, we explored the biological significance of pre-tRNA capping. Specifically, we developed capped short RNA sequencing (CaSh-seq), a method for comprehensively profiling small RNAs with 5′ cap structures. Using CaSh-seq, we systematically investigated capped pre-tRNAs in *S. cerevisiae* and found that nearly all pre-tRNAs undergo 5′ cap modification. Furthermore, this analysis enabled us to precisely determine TSSs of all tRNA genes for the first time, revealing that many tRNA genes have multiple TSSs. Additionally, we discovered that pre-tRNA capping is significantly upregulated under heat stress conditions. We also identified capped tRNA fragments derived from pre-tRNAs. Importantly, we demonstrated that capped pre-tRNAs interacted with eIF4E, thereby inhibiting cap-dependent translation. Our findings suggest that pre-tRNA capping acts as a temperature sensor to regulate cap-dependent translation under heat stress conditions.

Results

Heat stress promotes pre-tRNA capping in *S. cerevisiae*

To explore the biological significance of pre-tRNA capping, we examined whether pre-tRNA capping is affected by various environmental stresses. In our previous study[19], we demonstrated that capping enzymes exhibit a preference for pre-tRNAs with flexible 5′ leader sequences. Since heat stress is generally known to increase the structural flexibility of tRNAs[46], we hypothesized that pre-tRNA capping efficiency would be enhanced under heat stress. To test this, we cultured wild-type (WT) *S. cerevisiae* at 37 °C and monitored pre-tRNA capping under heat stress. Total RNAs were collected every hour, followed by immunoprecipitation (IP) using an anti-methyl-G cap antibody. IP products were analyzed by northern blotting (IP-northern) to detect specific pre-tRNAs (Fig. 1b). We chose two intronless tRNAs, $tRNA^{Arg}$ with UCU anticodon denoted tR(UCU), and $tRNA^{Gln}$ with UUG anticodon denoted tQ(UUG), along with one intron-containing $tRNA^{Trp}$ with CCA anticodon denoted tW(CCA). Following incubation at 37 °C,

https://doi.org/10.1038/s41467-026-76325-6

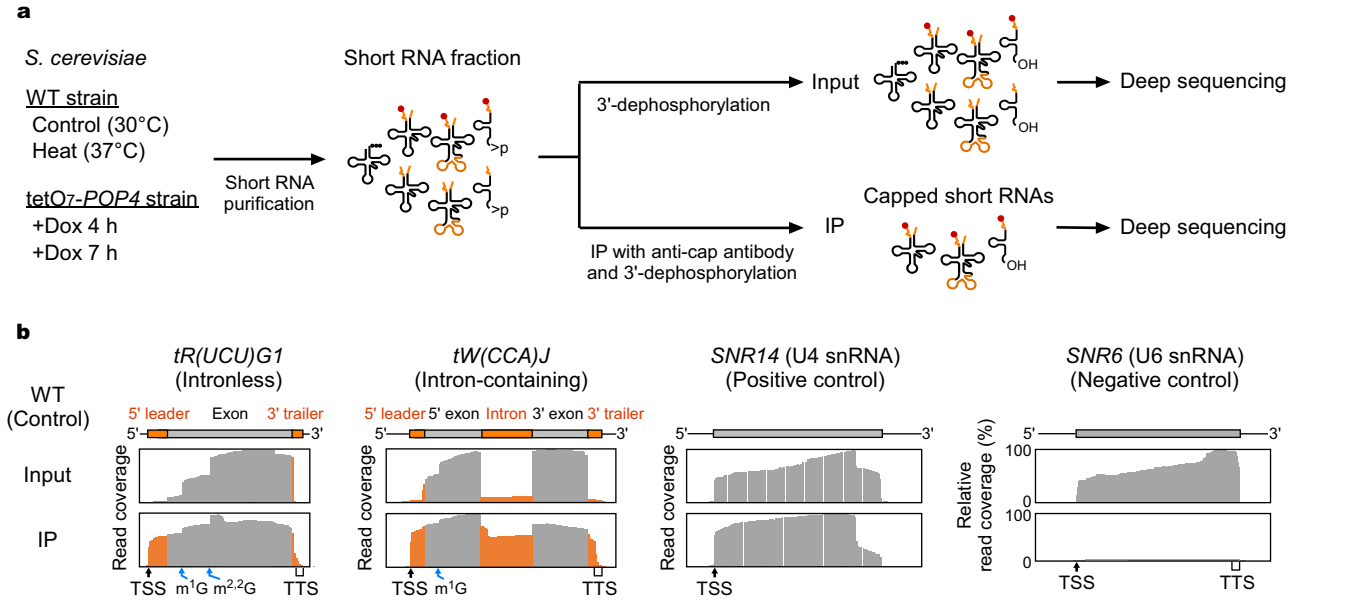

Fig. 2 | Comprehensive analysis of pre-tRNA capping in *S. cerevisiae* by CaSh-seq. a Schematic of CaSh-seq sample preparation. *S. cerevisiae* WT cells were cultured under control conditions (30 °C) or heat stress (37 °C) for 3.5 h. The tetO$_7$-*POP4* strain was cultured with Dox for 4 or 7 h. Short RNA fractions isolated from cells were either directly subjected to 3′-dephosphorylation (Input) or first enriched for capped RNAs via IP with anti-cap antibody, followed by 3′-dephosphorylation (IP). Both Input and IP samples were analyzed by deep sequencing. **b** CaSh-seq mapping results for four genes, *tR(UCU)G1*, *tW(CCA)J*, *SNR14* (U4 snRNA; positive control), and *SNR6* (U6 snRNA; negative control), along with their flanking regions in Input (upper) and IP (lower) samples from WT cells cultured under control conditions. Exons, 5′ leaders, 3′ trailers, and introns are shown in gray or orange. Gene structures are shown above, and transcription start and termination sites (TSS and TTS) are indicated by a black arrow and an open box, respectively. RT-stops caused by RNA modifications, N^1-methylguanosine (m^{1}G) and N^2,N^2-dimethylguanosine (m^{2,2}G), are indicated by blue arrows. Vertical axes represent read coverage or relative read coverage (%) normalized to *SNR14* for *SNR6*.

the capped precursor forms of tR(UCU) and tQ(UUG) gradually increased over 2–3 h but declined thereafter (Fig. 1b). Meanwhile, two precursor forms of tW(CCA) were observed; Type a (Pre 1a and 3a) with a long 5′ leader and Type b (Pre 1b and 3b) with a short 5′ leader[19]. Under normal conditions, Pre 1a/1b and a small amount of Pre 3a/3b were detected. However, after 4 h of heat stress, Type b precursors (Pre 1b and Pre 3b) were significantly increased (Fig. 1b). Notably, steady-state levels of mature tRNAs among total RNA (Input fraction) remained unchanged under heat stress conditions (Fig. 1b). Next, we examined pre-tRNA capping under different culture temperatures (30 °C, 34 °C, 37 °C, and 40 °C) after 3 h of incubation. The results showed that capped pre-tR(UCU) increased proportionally with temperature (Fig. 1c), while capped pre-tQ(UUG) and capped pre-tW(CCA) were relatively elevated at 40 °C (Fig. 1c).

Curiously, in addition to capped pre-tRNAs, we detected capped fragments of pre-tRNAs (5′ pre-tRFs) in the IP fraction. After 3 h of heat stress, capped 5′ pre-tRFs were detected from tR(UCU) and tW(CCA) but not from tQ(UUG) (Fig. 1b, c). Furthermore, levels of capped 5′ pre-tRFs increased with temperature but sharply declined at 40 °C (Fig. 1c). Generation of tRFs involves Rny1p, an RNase T$_2$ family member[47]. To investigate whether Rny1p is responsible for the production of capped 5′ pre-tRFs, we performed IP-northern blotting using the *rny1Δ* mutant strain. The results showed that in the absence of Rny1p, levels of capped 5′ pre-tRFs were significantly reduced under both normal and heat stress conditions (Fig. 1d). However, since some fragments were still detectable, it is likely that endonucleases other than Rny1p redundantly contribute to their generation (Fig. 1d). These findings suggest that Rny1p is the primary enzyme responsible for the production of capped 5′ pre-tRFs.

Taken together, our results demonstrate that heat stress not only enhances pre-tRNA capping in *S. cerevisiae* but also promotes the generation of capped 5′ pre-tRFs. However, their accumulation levels vary significantly depending on temperature, heat stress duration, and tRNA species.

Establishment of CaSh-seq

To comprehensively analyze capped pre-tRNAs, we developed CaSh-seq, a method that profiles capped short RNAs using deep sequencing approaches. The workflow for this method is illustrated in Fig. 2a. *S. cerevisiae* cells (WT) were cultured under normal growth conditions (30 °C; Control) and heat stress conditions (37 °C for 3.5 h; Heat). Total RNA was extracted, and short RNA fractions were prepared using anion-exchange chromatography (Input samples). Capped short RNAs (IP samples) were immunoprecipitated using K121 monoclonal antibody, which exhibits high affinity toward methylated guanosine cap structures and enables efficient enrichment of capped RNAs[19,48]. Following 3′-dephosphorylation, cDNA libraries of both the input and IP samples were prepared for deep sequencing. Since tRNAs contain diverse modifications that often inhibit reverse transcription, we used thermostable group II intron reverse transcriptase III (TGIRT-III), which has high processivity[49]. Sequencing reads were mapped to the *S. cerevisiae* S288C genome as a reference. Statistical summaries of CaSh-seq are provided in Supplementary Data 1 and 2.

To validate CaSh-seq, we conducted additional analyses using the tetO$_7$-*POP4* strain alongside WT cells. *POP4* is an essential factor for RNase P, and in this strain, transcription of *POP4* can be repressed by doxycycline (Dox), leading to accumulation of capped pre-tRNAs with 5′ leader sequences (Supplementary Fig. 2)[19,50]. In this study, tetO$_7$-*POP4* cells were cultured in the presence of Dox for 4 and 7 h, followed by CaSh-seq. Since capped pre-tRNAs are known to contain cap structures differing in methylation status[19], we confirmed that the anti-methyl-G cap antibody used in this study specifically and almost completely pulled down capped pre-tRNAs regardless of their methylation status using mass spectrometry (MS) (Supplementary Fig. 3a–c).

To illustrate the results of CaSh-seq, we mapped four representative genes in WT cells cultured under normal growth conditions (Fig. 2b). *SNR14* (U4 snRNA) as a positive control was clearly detected in the IP fraction due to its TMG cap, whereas *SNR6* (U6 snRNA) as a

negative control was absent in the IP fraction due to lack of a methyl-G cap, despite being detected in the Input fraction. The results confirmed that CaSh-seq accurately detected capped short RNAs. For *tR(UCU)G1* and *tW(CCA)J*, most sequencing reads in the Input fraction mapped to exon regions of the tRNA genes, with minimal mapping to extra regions including 5′ leader, 3′ trailer, and introns (Fig. 2b). By contrast, in the IP fraction, significantly more reads mapped to the extra regions (Fig. 2b). These findings suggest that capped pre-tRNAs were efficiently enriched in the IP fraction, whereas mature tRNAs and end-matured pre-tRNAs were effectively removed. Furthermore, CaSh-seq mapping clearly identified the TSSs and TTSs of individual tRNA genes (Fig. 2b). We also observed pronounced coverage drops at specific positions within tRNA exons that correspond to known modification sites (Fig. 2b and Supplementary Fig. 4). These drops are attributable to RT stops induced by N^1-methylguanosine (m^1G) and N^2,N^2-dimethylguanosine ($m^{2,2}G$) modifications[51,52]. In the tetO$_7$-*POP4* strain, tRNA-mapping reads were markedly higher in IP samples than in the WT strain, with the most prominent accumulation observed after 7 h of Dox treatment (Supplementary Fig. 5 and Supplementary Data 2). CaSh-seq also detected 5′ region of the capped mRNAs including their precursors and degradation products (Supplementary Fig. 6 and Supplementary Data 2).

Taken together, these findings demonstrate that CaSh-seq is a reliable and effective method for profiling capped pre-tRNAs, providing a robust tool for investigating pre-tRNA capping dynamics.

Widespread pre-tRNA capping and comprehensive TSS mapping

The *S. cerevisiae* genome encodes 275 tRNA genes, among which eight are bicistronic tRNA genes [*tR(UCU)–tD(GUC)*] (Supplementary Fig. 4)[53]; therefore, the actual number of distinct tRNA genes is 271. Although 267 tRNA genes were transcribed according to CaSh-seq data, transcripts of four genes [*tK(CUU)C*, *tL(CAA)C*, *tM(CAU)C*, and *tD(GUC)N*] were not detected, suggesting they are either inactive or deleted in the strains[54,55]. From CaSh-seq analysis of the tetO$_7$-*POP4* strain, pre-tRNAs derived from 267 tRNA genes were detected in the IP fraction, demonstrating that all pre-tRNAs expressed in *S. cerevisiae* undergo cap modification.

Based on the marked reduction in mapped reads, we comprehensively explored the TSSs and TTSs of each tRNA gene, successfully identifying both for 267 tRNA genes at single-nucleotide resolution (Supplementary Data 3–5). According to previous studies[16,18,56], RNAPIII initiates transcription at the purine residue of the pyrimidine-purine (Py-Pu) motif of TSSs. Intriguingly, multiple TSSs were predicted in many tRNA genes. TTSs are defined as sites with five or more consecutive thymidine residues (Supplementary Data 4). As previously reported[17], we observed readthrough of transcription termination at the typical TTSs in *tH(GUG)G2* and *tK(UUU)O* (Supplementary Fig. 7a). Additionally, under heat stress conditions, 3′ trailer sequences of pri-tRNAs were extended in *tI(UAU)D* and *tK(UUU)D*[10] (Supplementary Fig. 7b).

CaSh-seq detected multiple TSSs in a number of tRNA genes (Fig. 3a and Supplementary Data 3, 5). As an example, in the *tI(AAU)I2* gene, a marked decrease in read counts was observed at positions −11A and −13A from the 5′ processing site (5′PS) in IP samples of both WT and tetO$_7$-*POP4* strains, suggesting the presence of two TSSs (Fig. 3a). To validate this observation, pre-tI(AAU) was isolated from the tetO$_7$-*POP4* strain, digested with RNase T$_1$, and analyzed by MS to examine 5′-terminal RNA fragments (Fig. 3b). We clearly detected 5′-capped fragments from mono-, di-, and tri-methylguanosines derived with pre-tRNAs transcribed from both −11A and −13A positions (Fig. 3b). Based on this finding, we explored tRNA genes with multiple TSSs using CaSh-seq data. We identified 36 tRNA genes with two TSSs and one gene with three TSSs (Supplementary Data 3, 5). In tRNA genes bearing a single TSS, the TSSs were primarily distributed at positions −9 to −12 from the 5′PS, with an average length for the 5′ leader of 10.4 ± 1.4 nucleotides (Fig. 3c). Sequence logos of the TSSs clearly showed the CA motif at positions −1 and +1 (Fig. 3d). Oligo T and A stretches were observed upstream and downstream of TSSs, respectively (Fig. 3d).

On the other hand, in tRNA genes with multiple TSSs, the TSSs are more widely distributed, primarily at positions −8 to −13 from the 5′PS, with an average length for the 5′ leader of 10.0 ± 2.2 nucleotides (Fig. 3c). The spacing between TSSs varied (Supplementary Data 3, 5), with the most common interval being two nucleotides (15/36 genes), followed by three nucleotides (14/36 genes). Sequence logos of multiple TSSs spaced two nucleotides apart clearly showed Py-Pu motifs but less conservation of the CA motif at both sites (Fig. 3d).

Curiously, TSS usage was altered in a few tRNA genes under heat stress (Fig. 3e, f and Supplementary Data 3). Two tRNA genes with multiple TSSs, *tS(UGA)I* and *tL(CAA)G1*, exhibited large TSS changes from upstream to downstream sites following heat stress (Fig. 3e, f and Supplementary Data 3). These observations raise the possibility that heat stress may influence TSS selection by RNAPIII; alternatively, it may affect the capping efficiency or processing speed of pre-tRNAs.

In summary, RNAPIII strongly selects the CA motif of TSSs at positions −9 to −12 from the 5′PS. However, in the absence of such characteristics, RNAPIII flexibly selects suboptimal Py-Pu motifs of multiple TSSs. Overall, CaSh-seq provides comprehensive insights into tRNA transcription and maturation dynamics. Capturing even low-abundance primary transcripts by CaSh-seq enables analysis of tRNA maturation in its early stages.

Pre-tRNA capping stabilizes unstable tRNA precursors under heat stress

To characterize changes in pre-tRNA capping under heat stress conditions, we classified pre-tRNAs and 5′ pre-tRFs into distinct groups by using tag codes (Supplementary Fig. 8 and Supplementary Data 6). Under normal growth conditions, capped pre-tRNAs detected in both Input and IP fractions were predominantly classified as Pre, followed by Pre 1 and Pre 3 species (Fig. 4a and Supplementary Data 6, 7). In addition, 5′ pre-tRFs generated from nearly all pre-tRNAs constituted the second most abundant class of capped molecules (Fig. 4a, Supplementary Fig. 9 and Supplementary Data 6, 7). Upon heat stress, the overall abundance of capped pre-tRNAs increased, with a particularly pronounced enrichment of the Pre 3 class in the IP fraction (Fig. 4a and Supplementary Data 7), suggesting preferential stabilization of specific pre-tRNA intermediates under stress conditions.

To quantitatively assess the relative extent of pre-tRNA capping across individual tRNA genes, we defined a cap score parameter (Supplementary Fig. 10). The cap score was calculated as the ratio of IP reads to Input reads for each pre-tRNA, normalized to the IP/Input ratio of U4 snRNA, which is constitutively capped. In the Input datasets, we analyzed pre-tRNAs with at least five reads mapped to their 5′ leader regions. Using this approach, cap scores were obtained for 254 tRNA genes under normal conditions and for 183 genes under heat stress in WT cells. In tetO$_7$-*POP4* strains, cap scores were calculated for 267 and 265 genes following 4 h and 7 h Dox treatment, respectively (Supplementary Data 8).

Cap scores varied substantially among different tRNA species (Supplementary Fig. 11a, b), indicating that intrinsic features of pre-tRNA sequences and structures influence their propensity for capping and/or their stability once capped. Importantly, the cap score does not represent an absolute measure of capping efficiency. Rather, it serves as a relative index reflecting steady-state capping propensity, as it is derived from relative read counts and assumes comparable immunoprecipitation efficiency across RNA species.

In our previous study[19], we directly quantified absolute capping efficiencies for several isolated pre-tRNAs using LC–MS and demonstrated that, under normal growth conditions in WT cells, approximately 5–22% of pre-tRNAs are capped. To relate these absolute values to the cap scores obtained by CaSh-seq, we compared cap scores

https://doi.org/10.1038/s41467-026-76325-6

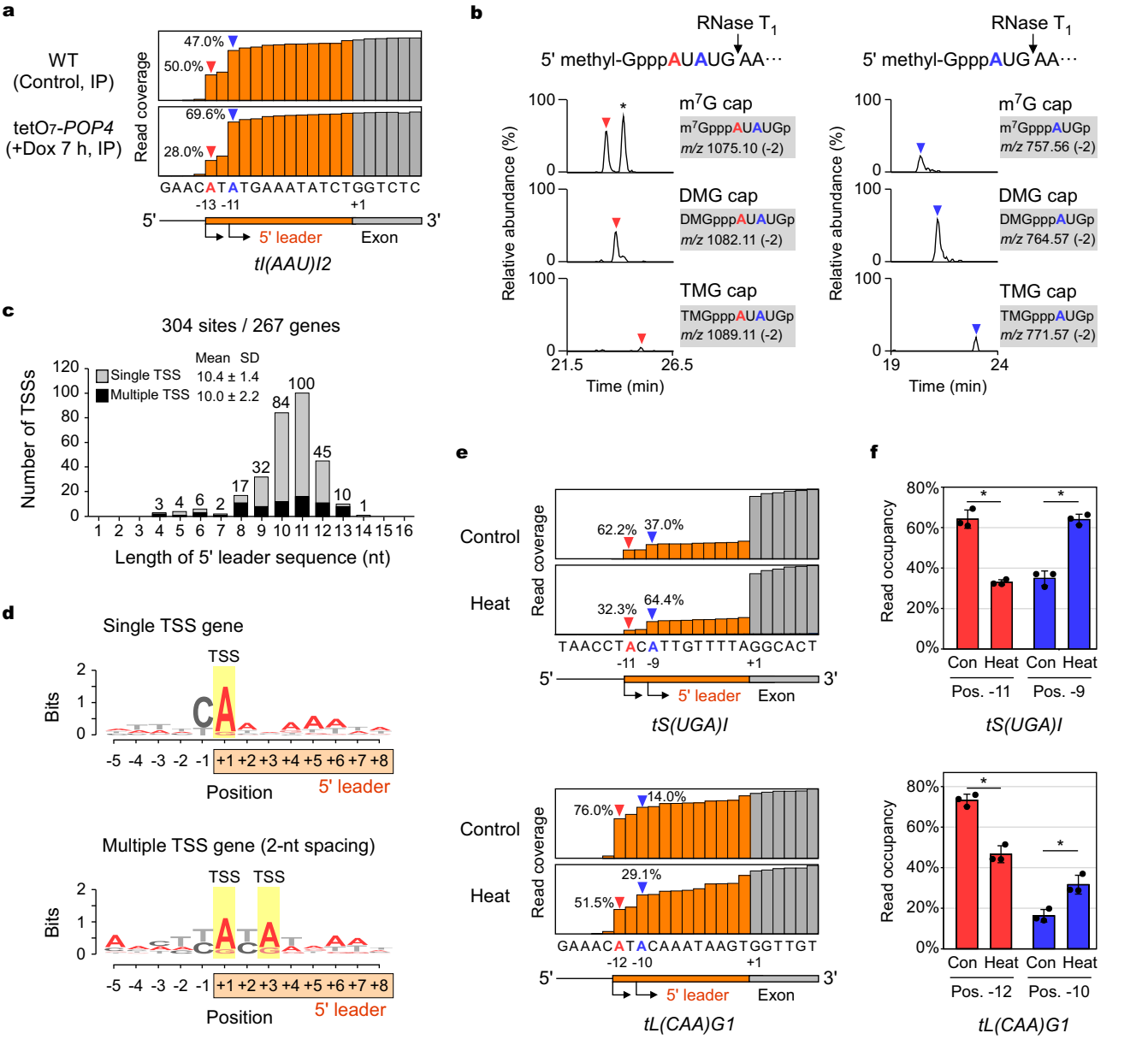

Fig. 3 | TSS mapping of *S. cerevisiae* tRNA genes by CaSh-seq. a CaSh-seq mapping results for the 5′ leader region of *tI(AAU)I2* in IP samples from WT (control, upper) and tetO$_7$-*POP4* (+Dox 7 h, lower) strains. Gene structure and genomic sequence are shown below. Reduced read coverage at −13A and −11A is indicated by red and blue arrowheads and letters. Read occupancy at individual TSSs is also shown. **b** LC/MS analysis of 5′ capping of pre-tI(AAU) from tetO$_7$-*POP4* cells. Shown are extracted ion chromatograms (XICs) of RNase T$_1$-digested 5′ fragments containing m^{7}G, DMG, or TMG caps, transcribed from −13A (left) and −11A (right) TSSs. Peaks are indicated by colored arrows corresponding to (**a**). Vertical axes represent relative peak intensities, normalized to the total signal intensity of the fragments. An asterisk (*) indicates an unassigned ion. LC/MS analysis was performed once for each sample. **c** Distribution of 5′ leader lengths among 267 tRNA genes. The x-axis shows the length of 5′ leader sequence (nucleotides, nt) and the y-axis indicates the number of TSSs. TSSs from single-TSS genes (231 TSSs) and multiple-TSS genes (73 TSSs) are shown in gray and black, respectively. Means with standard deviation (SD) values are indicated. **d** Sequence logos spanning −5 to +8 relative to the TSS (+1) for single-TSS genes (upper) and for multiple-TSS genes with 2-nt spacing (lower). TSSs and 5′ leader regions are highlighted in yellow and orange, respectively. Sequence logos were generated using WebLogo 3[99]. **e** CaSh-seq mapping results for 5′ leader regions of *tS(UGA)I* (upper) and *tL(CAA)G1* (lower) in IP samples from WT cells under control (upper) or heat-stress (lower) conditions. Displayed as in (**a**). **f** Bar graphs showing read occupancy at each TSS with indicated positions of *tS(UGA)I* (upper) and *tL(CAA)G1* (lower) in IP samples from WT cells control (left) or heat-stress (right) conditions. Results are means ± SD from three biological replicates. Asterisks (*) indicate statistically significant differences, determined by a two-sided Welch's t-test. Exact *p* values were: *tS(UGA)I*, 0.0043 (Pos. −11) and 0.0006 (Pos. −9); *tL(CAA)G1*, 0.0013 (Pos. −12) and 0.0124 (Pos. −10). Source data are provided as a Source Data file.

(Supplementary Data 8) with LC–MS–determined capping frequencies for four representative pre-tRNAs, tL(UAG), tL(CAA), tW(CCA)_a, and tW(CCA)_b (Supplementary Fig. 12a). Cap scores showed a strong positive correlation with LC–MS-based capping efficiencies ($R^2 = 0.97$), indicating that the cap score provides a reliable surrogate measure of relative capping frequency (Supplementary Fig. 12a). These reference pre-tRNAs collectively span nearly the full dynamic range of cap scores observed among the 263 tRNA genes for which Pre or Pre1 cap scores could be calculated in WT cells, supporting the applicability of this calibration across the tRNA gene set (Supplementary Fig. 12b and Supplementary Data 8).

To determine whether 5′ capping is established at the earliest stages of tRNA biogenesis, we extended our analysis to pri-tRNAs. Using tag codes corresponding to the oligo-U sequence at the 3′ trailer

https://doi.org/10.1038/s41467-026-76325-6

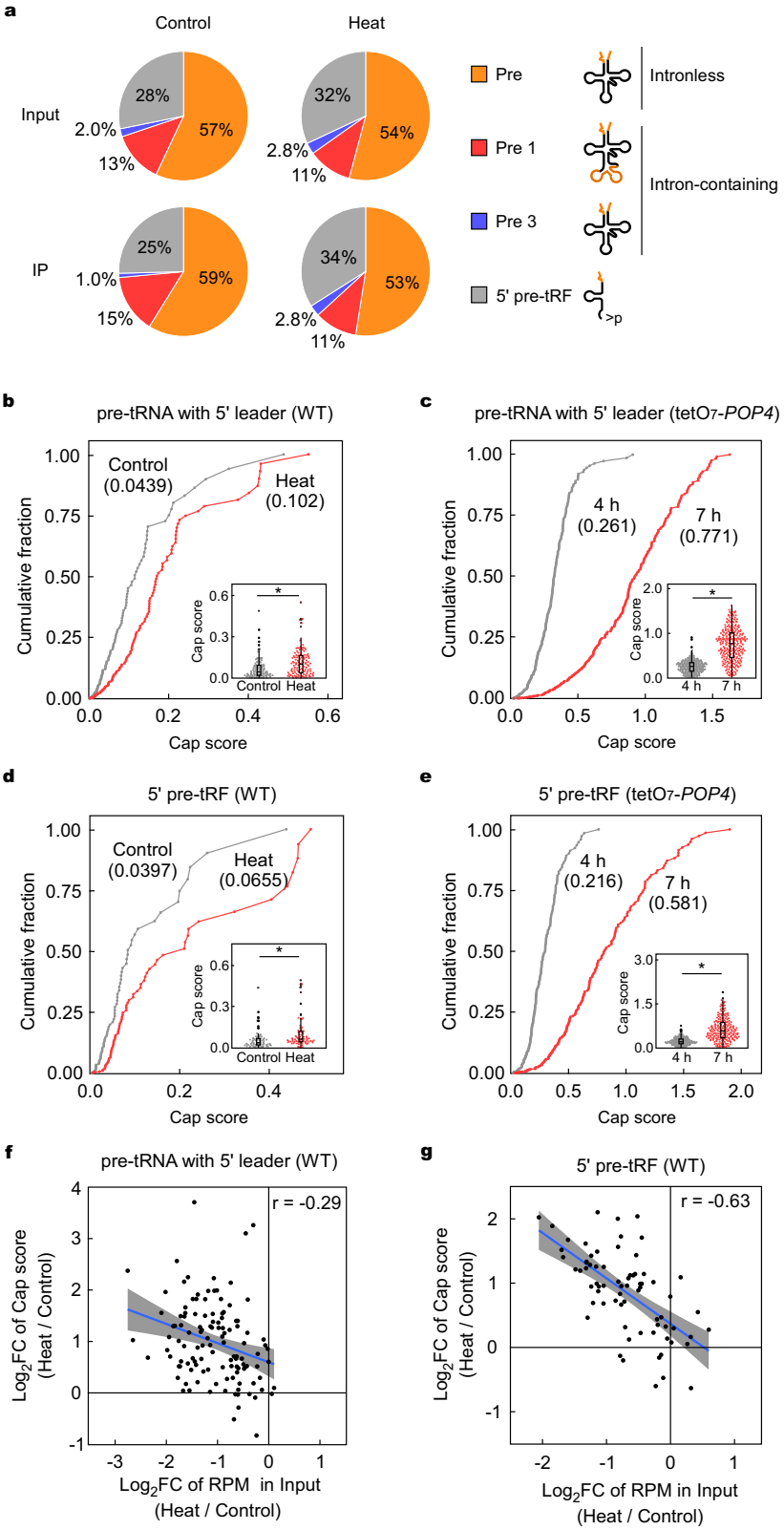

termini (Supplementary Fig. 8), we selectively extracted pri-tRNAs from WT CaSh-seq datasets obtained under normal growth conditions and calculated cap scores for 136 tRNA genes (Supplementary Data 8). Comparison of cap score distributions revealed that pri-tRNAs exhibited slightly lower median cap scores and a narrower distribution than pre-tRNAs (Pre and Pre 1) (Supplementary Fig. 12c), indicating that 5′ capping is already introduced at or shortly after transcription initiation and that capped molecules become relatively enriched during subsequent processing from pri- to pre-tRNAs. Based on LC–MS-based calibration of cap scores, we estimate that pri-tRNAs and pre-tRNAs (Pre and Pre 1) are capped at average steady-state frequencies of 6.3 ± 0.7% (n = 136) and 8.2 ± 1.4% (n = 263), respectively

Fig. 4 | Heat stress-induced alterations in the capping of pre-tRNAs and 5′ pre-tRFs. a Pie charts showing the relative abundance of each pre-tRNA species and 5′ pre-tRF in Input (upper panels) and IP (lower panels) samples from WT cells cultured under control (left) or heat stress (right) conditions. Each species is color-coded and illustrated as indicated on the right. **b**–**e** Cumulative distribution plots of cap scores for pre-tRNAs with 5′ leaders (Pre, Pre 1, and Pre 3) (**b**,**c**) and for 5′ pre-tRFs (**d**,**e**) in WT cells under control versus heat stress conditions (**b**,**d**), or in tetO$_7$-*POP4* cells treated with Dox for 4 h versus 7 h (**c**,**e**). Insets show corresponding swarm and box plots, displaying the median (center line), the interquartile range (bounding box), the 1.5 interquartile range (whiskers), and outliers (black dots). Results represent mean from three biologically independent experiments. Asterisks (*) denote statistically significant differences based on a two-sided Mann-Whitney U test with Bonferroni correction for multiple comparisons. Exact *p* values were: b, 1.01e−05; c, 2.2e−16; d, 2.34e−04; e, 2.2e−16). **f**,**g** Scatter plots comparing the log$_2$ fold change (Log$_2$FC) in reads per million (RPM) of pre-tRNAs with 5′ leaders (Pre, Pre 1, and Pre 3) (**f**) and 5′ pre-tRFs (**g**) in Input samples under heat stress versus control conditions, plotted against the corresponding Log$_2$FC of the cap scores. Blue lines indicate linear regression fits; shaded areas represent the 95% confidence intervals of the fitted regression lines. Correlation coefficients of the plots with r = −0.29 (**f**) and r = −0.63 (**g**), respectively. Source data are provided as a Source Data file.

(Supplementary Fig. 12c). Together, these results support a model in which 5′ capping is introduced early during RNAPIII transcription and subsequently contributes to the selective stabilization and accumulation of otherwise unstable tRNA precursor intermediates, particularly under heat stress conditions. Importantly, these values reflect steady-state capping efficiencies and do not directly report the fraction of newly synthesized tRNA precursors that acquire caps immediately upon transcription.

The median cap scores of pre-tRNAs in WT cells were 0.0439 under normal conditions and 0.102 under heat stress (Fig. 4b). Cumulative plots revealed a significant increase in cap scores of pre-tRNAs under heat stress conditions (Fig. 4b, Supplementary Fig. 11a, and Supplementary Data 8). In tetO$_7$-*POP4* strains, the overall cap scores were higher than those in WT cells (Fig. 4b, c and Supplementary Fig. 11a, b, Supplementary Data 8), and a notable increase in cap score was observed in the 7 h Dox-treated sample compared with the 4 h-treated sample (Fig. 4c, Supplementary Fig. 11b and Supplementary Data 8). These results are consistent with those of Northwestern blotting of capped RNAs (Supplementary Fig. 2), clearly demonstrating a positive correlation between capped pre-tRNA accumulation and capping efficiency.

The cap scores of 5′ pre-tRFs also increased under heat stress conditions (Fig. 4d and Supplementary Fig. 13a and Supplementary Data 8) as well as upon RNase P inhibition (Fig. 4e and Supplementary Fig. 13b, Supplementary Data 8). Curiously, there were no correlations between the cap scores of 5′ pre-tRFs and those of their corresponding pre-tRNAs (Supplementary Data 8), indicating that production of capped 5′ pre-tRFs is likely due to the substrate specificity of Rny1p (Fig. 1d).

Given the weak negative correlation observed between the cap score and the steady-state level of each pre-tRNA (Supplementary Fig. 14a, b), we hypothesized that pre-tRNA capping may stabilize unstable pre-tRNAs. To test this hypothesis, we analyzed the relationship between changes in cap scores and steady-state levels in Input samples for each pre-tRNA under normal and heat stress conditions in WT strains. This analysis revealed a weak negative correlation for pre-tRNAs (r = −0.29) (Fig. 4f), with a similar but stronger trend observed for 5′ pre-tRFs (r = −0.63) (Fig. 4g). These findings suggest an association between the 5′ capping and unstable pre-tRNAs and 5′ pre-tRFs, which may reduce their degradation by 5′ exonucleases, particularly under heat stress conditions.

Pre-tRNA capping tends to occur on flexible 5′ leaders

In our previous study, we proposed that the frequency of pre-tRNA capping is influenced by the terminal secondary structure formed by 5′ leader and 3′ trailer sequences[19]. To further investigate this finding, we selected three pri-tRNAs with the highest cap scores and three with the lowest cap scores from 4 h Dox-treated tetO$_7$-*POP4* strains, and compared the stability of their terminal secondary structures by calculating the base-pairing probability at the 5′ terminus of each pri-tRNA using CentroidFold[57] (Supplementary Data 9). The results showed that the three pri-tRNAs with high cap scores all exhibited low base-pairing probabilities at the 5′ terminus (0.0094–0.0286), indicating that their 5′ leaders are predominantly single-stranded (Supplementary Fig. 15). By contrast, the three pri-tRNAs with low cap scores had high base-pairing probabilities at the 5′ terminus (0.2758–0.3447), forming a double-stranded 5′ leader (Supplementary Fig. 15). These findings suggest that pre-tRNAs bearing single-stranded 5′ leaders are capped efficiently, whereas those prone to forming double-stranded 5′ leaders are less likely to undergo capping.

To further examine this trend comprehensively, we calculated the base-pairing probability at the 5′ terminus for each pri-tRNA using CentroidFold (Supplementary Data 9), and compared these probabilities with the cap scores in the tetO$_7$-*POP4* strain treated with Dox for 4 and 7 h (Fig. 5a). According to their base-pairing probabilities, all analyzed pri-tRNAs were classified into three groups: low probability (<0.05), medium probability (0.05–0.2), and high probability (> 0.2). Distributions of cap scores were compared among these groups, showing that higher base-pairing probabilities correlated with lower cap scores under both conditions (Fig. 5a and Supplementary Data 8, 9).

The proportion of pre-tRNAs without 3′ trailers was higher in 7 h Dox-treated samples than in 4 h Dox-treated samples (Supplementary Fig. 16 and Supplementary Data 6). To further examine this, pre-tRNAs were categorized into three types (Pre, Pre 1, and Pre 3) and their cap scores were compared between those with and those without 3′ trailers. We found that removal of the 3′ trailer significantly increased the cap score in all cases (Fig. 5b). These results indicate that 3′ trailer removal enhances 5′ leader flexibility, thereby facilitating pre-tRNA capping.

Pre 3 species consistently exhibited higher cap scores than Pre 1 molecules, regardless of the presence or absence of the 3′ trailer (Fig. 5b, Supplementary Fig. 17, and Supplementary Data 8). These findings are consistent with our previous study showing that Pre 3 species have higher capping efficiency and methylation status than Pre 1 molecules[19]. Given that pre-tRNAs in the alternative pathway travel a long distance in the cell, Pre 3 species have more opportunities to undergo 5′ capping. In addition, 5′ capping is required to stabilize Pre 3 molecules by protecting them from exonucleolytic degradation until removal of the 5′ leader by RNase P.

Taken together, these results demonstrate that flexibility of the 5′ leader directly influences the efficiency of pre-tRNA capping.

Capped pre-tRNAs modulate cap-dependent translation

To investigate the biological functions of capped pre-tRNAs, we examined interactions between capped pre-tRNAs and cap-binding proteins in the cell. Two cap-binding proteins are present in *S. cerevisiae*[40]. Cbc2p is a nuclear cap-binding protein that forms a heterodimer with Cbc1p and is involved in promoting mRNA splicing, nuclear export of mRNA, and mediating the pioneer round of cap-dependent translation[43]. eIF4E is a translation initiation factor localized to the cytoplasm that plays an essential role in cap-dependent translation[58]. We expressed FLAG-tagged eIF4E or Cbc2p in the tetO$_7$-*POP4* strain. After accumulation of pre-tRNAs following Dox treatment, cells were crosslinked with formaldehyde, and each cap-

https://doi.org/10.1038/s41467-026-76325-6

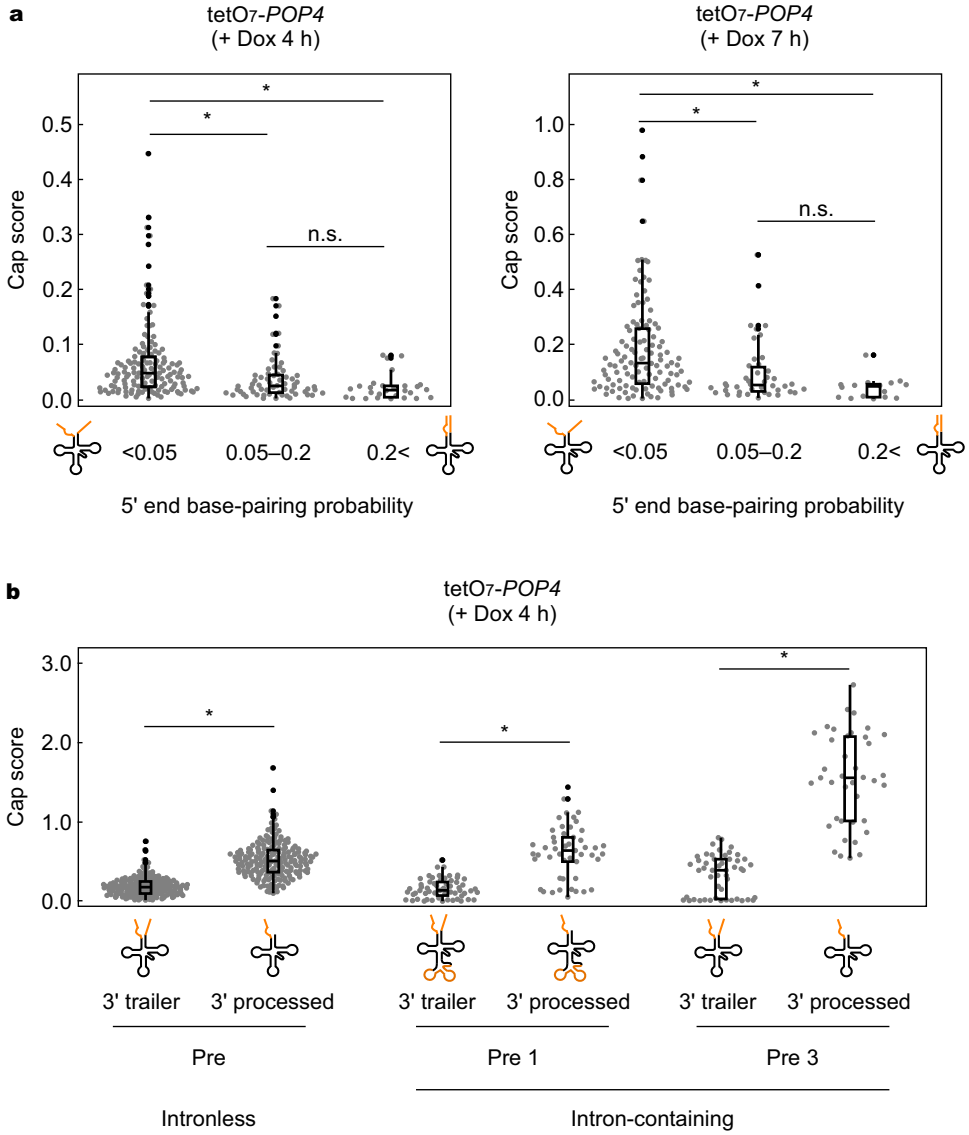

Fig. 5 | Pre-tRNA capping preferentially occurs at flexible 5′ leaders. **a** Comparison of cap scores based on base-pairing probabilities at the 5′ ends of pri-tRNAs in the tetO$_7$-*POP4* strain cultured with Dox for 4 h (left) or 7 h (right). Pri-tRNAs were grouped into three categories according to their 5′ end base-pairing probability (Supplementary Data 9): low (<0.05), medium (0.05–0.2), and high (>0.2). Data are represented as swarm plots with overlaid box plots, displaying the median (center line), the interquartile range (bounding box), the 1.5 interquartile range (whiskers), and outliers (black dots). Results represent mean from three biologically independent experiments. Asterisks (*) indicate statistically significant differences; "n.s." denotes non-significant differences. Statistical significance was determined by a two-sided Mann-Whitney U test with Bonferroni correction. Exact *p* values were: low vs medium, 1.05e−04; low vs high, 2.17e−06; medium vs high, 0.0227 (4 h); low vs medium, 3.68e−04; low vs high, 2.37e−05; medium vs high, 0.0518 (7 h). **b** Comparison of cap scores among different pre-tRNA species in the 4 h Dox-treated tetO$_7$-*POP4* strain: Pre from intronless tRNA genes, and Pre 1 and Pre 3 from intron-containing tRNA genes, categorized by the presence of a 3′ trailer sequence (3′ trailer) or a processed/matured 3′ end (3′ processed). Data are represented as swarm plots with overlaid box plots, displaying the median (center line), the interquartile range (bounding box), the 1.5 interquartile range (whiskers), and outliers (black dots). Asterisks (*) indicate statistically significant differences, determined by a two-sided Mann-Whitney U test with Bonferroni correction. Exact *p* values were: Pre, <2.2e−16; Pre 1, 6.78e−12; Pre 3, 8.37e−06. Source data are provided as a Source Data file.

binding protein was immunoprecipitated with an anti-FLAG antibody (Supplementary Fig. 18). Northern blotting analysis of the co-precipitates revealed that pre-tI(AAU) with 5′ leader was enriched in the eIF4E IP fraction upon crosslinking (Fig. 6a). By contrast, only a small amount of this pre-tRNA was detected in the Cbc2 IP fraction (Fig. 6a). These results suggest that capped pre-tRNAs preferentially bind to eIF4E rather than to Cbc2p. We also performed northern blotting for four intron-containing tRNAs and detected Pre 1 and Pre 3 species in the crosslinked IP fraction (Fig. 6b). Compared to Pre 1, Pre 3 was more prominently detected in all cases, suggesting that Pre 3, which is a post-splicing precursor predominantly localized to the cytoplasm, binds to eIF4E in the cytoplasm.

Next, co-precipitates with eIF4E were further immunoprecipitated with an anti-cap antibody, followed by northern blotting to detect pre-tI(UAU). Pre 1 and Pre 3 species were clearly detected in the IP fraction, whereas mature tRNAs contaminating the co-precipitant were detected in the flowthrough fraction (Fig. 6c). These findings strongly indicate that pre-tRNA directly interacts with eIF4E via the cap structure.

We subsequently examined whether capped pre-tRNAs sequester eIF4E and thereby inhibit cap-dependent translation. The capped pre-tRNAs were prepared from the tetO$_7$-*POP4* strain (Fig. 6d). To make a negative control, a portion of the capped pre-tRNAs were decapped chemically (Fig. 6d and Supplementary Fig. 19a). We measured cap-

https://doi.org/10.1038/s41467-026-76325-6

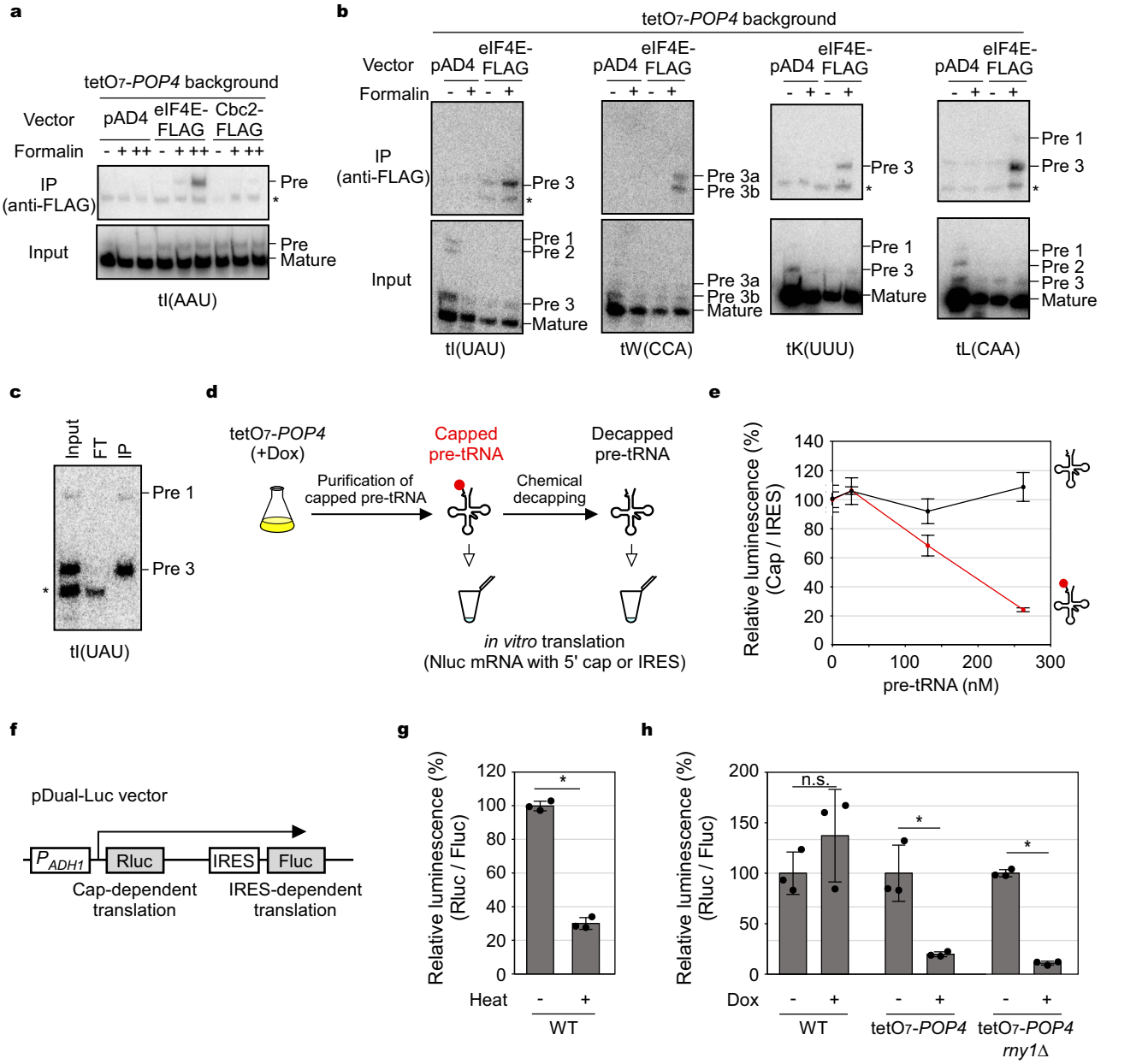

Fig. 6 | Modulation of cap-dependent translation by sequestration of eIF4E with capped pre-tRNAs. a Northern blotting of RNAs from whole-cell extracts (Input) and corresponding FLAG-IPed fractions of tetO$_7$-*POP4* strains carrying pAD4 (empty vector), Cbc2-FLAG, or eIF4E-FLAG. A probe against tI(AAU) was used to detect mature and pre-tRNA species. Asterisks (*) indicate contaminating mature tRNA. "–", "+", and "++" represent formaldehyde crosslinking at 0%, 0.005%, and 0.02%, respectively. Similar results were obtained in multiple independent experiments. **b** Northern blotting of RNAs shown in (a), using probes against tI(UAU), tK(UUU), tL(CAA), and tW(CCA). "–" and "+" indicate the absence or presence of crosslinking. **c** Northern blotting following sequential immunoprecipitation: RNAs from the eIF4E-FLAG IP fraction (**a**) were subjected to a second IP using anti-cap antibody. Input, flowthrough (FT), and IP fractions were analyzed using a probe against tI(UAU). **b**,**c** represent experiments performed once. **d** Schematic of the in vitro translation assay. Capped pre-tRNAs purified from tetO$_7$-*POP4* cells were either left untreated or subjected to chemical decapping. These samples were added to an in vitro translation system along with in vitro-synthesized Nluc mRNA with 5′ cap or IRES. **e** In vitro translation assay using RRL. Line graphs show cap-dependent Nluc activity normalized to IRES-dependent Nluc (%) in reactions containing capped (red) or decapped pre-tRNA (black) at increasing concentrations. Luminescence without pre-tRNAs was set to 100%. Results are presented as mean ± SD from three technical replicates. **f** Schematic of the pDual-Luc vector. Bicistronic mRNA, expressed under the *ADH1* promoter (P_{ADH1}), encodes Rluc (cap-dependent translation) and Fluc (IRES-dependent translation). **g**,**h** In vivo dual luciferase reporter assay. Bar graphs show relative luminescence (Rluc/Fluc) in WT strain cultured with (+) or without (−) heat stress (37 °C, 3.5 h) (**g**) or WT, tetO$_7$-*POP4*, and tetO$_7$-*POP4 rny1*Δ strains cultured with (+) or without (−) Dox for 7 h (**h**). Values without heat stress or Dox were set to 100%. Results are presented as mean ± SD from three biological replicates. Statistical significance was determined by a two-sided Welch's t-test. Exact *p* values were: **g** 2.0e−05; **h** 0.29697 (WT); 0.03697 (tetO$_7$-*POP4*), and 3.0e−05 (tetO$_7$-*POP4 rny1*Δ). Source data are provided as a Source Data file.

dependent translation of nano luciferase (Nluc) mRNA in vitro (Fig. 6d). To assess specific inhibition of cap-dependent translation by the capped pre-tRNAs, we prepared an Nluc reporter driven by cricket paralysis virus (CrPV) internal ribosome entry site (IRES) as a negative control[59,60]. We performed in vitro translation of both the cap-dependent Nluc reporter and the CrPV-IRES–dependent Nluc reporter using rabbit reticulocyte lysate (RRL), and directly compared the effects of capped pre-tRNAs on these two modes of translation. The

https://doi.org/10.1038/s41467-026-76325-6

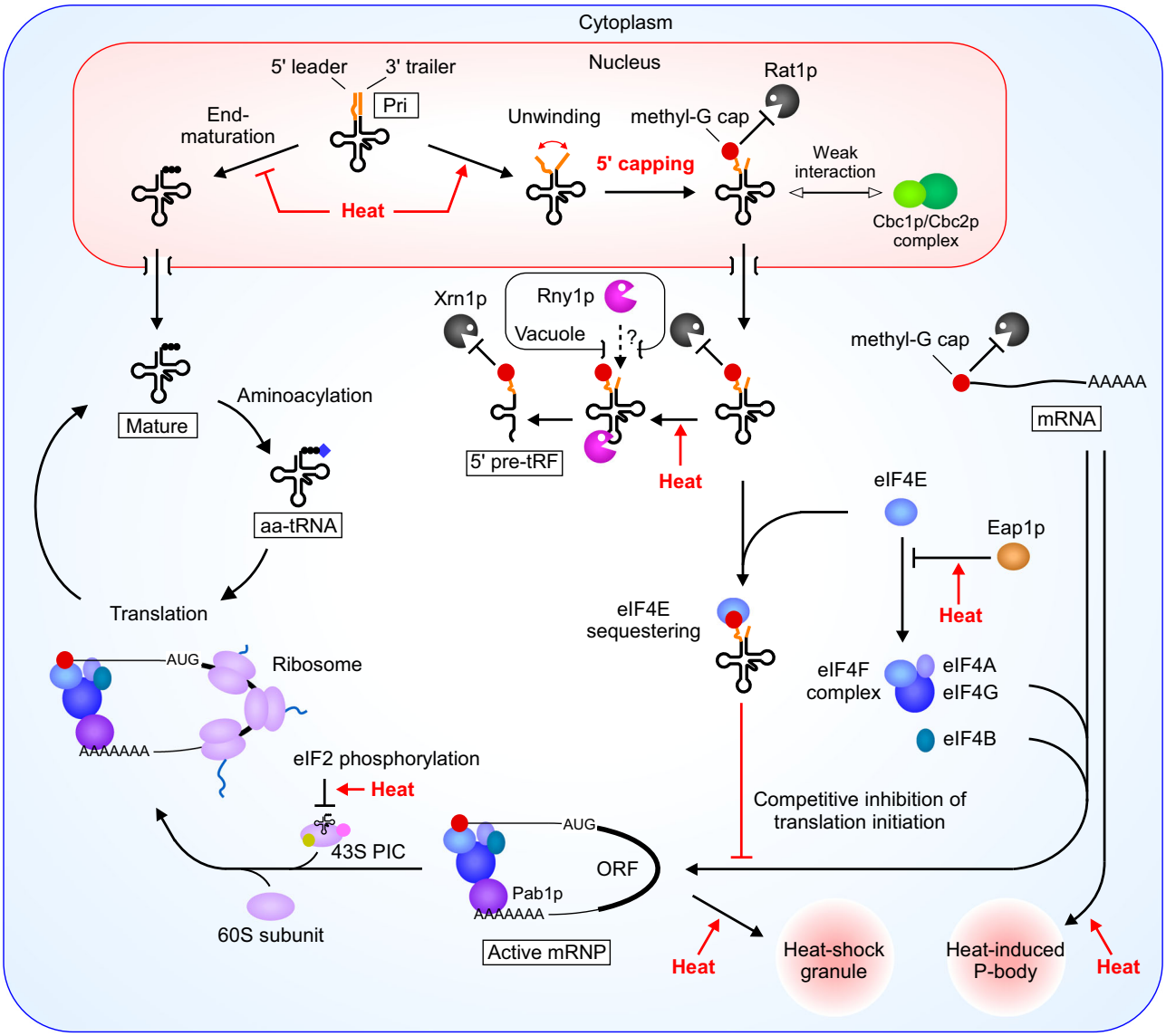

Fig. 7 | Proposed regulatory role of pre-tRNA capping in translation initiation under heat stress. In rapidly growing cells, tRNAs and proteins are efficiently produced. Under heat stress conditions, the 5′ leader sequences of pre-tRNAs become more flexible, facilitating addition of methylguanosine caps (red circles), which might protect unstable pre-tRNAs from 5′-to-3′ exonucleolytic degradation. In the cytoplasm, the capped pre-tRNAs compete with mRNAs for binding to eIF4E. Sequestration of eIF4E by capped pre-tRNAs would contribute to modulation of cap-dependent translation and may promote P-body formation, where mRNA decay occurs. Heat stress also enhances Rny1p-mediated cleavage of capped pre-tRNAs, generating capped 5′ pre-tRNA fragments (pre-tRFs). These capped fragments may similarly suppress cap-dependent translation (indicated by dashed lines). In parallel, translation initiation is broadly inhibited under heat stress through multiple pathways, including eIF2 phosphorylation, inhibition of eIF4F function by Eap1p, and sequestration of untranslated mRNPs into heat-shock granule. In the nucleus, capped pre-tRNAs interact weakly with the Cbc1/Cbp20-Cbp80 (Cbc1/Cbc2) complex, which may affect the regulation or processing of other capped RNAs.

addition of capped pre-tRNAs markedly reduced translation of the cap-dependent Nluc mRNA compared with IRES-dependent Nluc translation under the same conditions (Fig. 6e). In contrast, the decapped pre-tRNAs did not cause a significant reduction in translation of either reporter (Fig. 6e). Furthermore, similar analyses were conducted using a wheat germ extract–based translation system. The addition of capped pre-tRNAs resulted in a dose-dependent reduction in the translation activity of the cap-dependent Nluc reporter (Supplementary Fig. 19b). By contrast, chemically decapped pre-tRNAs showed no inhibitory activity at any of the concentrations tested (Supplementary Fig. 19b). These results indicate that capped pre-tRNAs preferentially and more strongly inhibit cap-dependent translation relative to IRES-mediated translation, supporting a selective role for capped pre-tRNAs in repressing cap-dependent protein synthesis.

Finally, we investigated whether capped pre-tRNAs inhibit cap-dependent translation in yeast cells using a dual luciferase reporter assay. We evaluated cap-dependent translation of *Renilla* luciferase (Rluc) (Fig. 6f). As an internal control, CrPV-IRES-dependent translation of firefly luciferase (Fluc) was measured (Fig. 6f). Upon heat stress treatment, the Rluc/Fluc ratio decreased to approximately 30% of the control level under heat stress (Fig. 6g). These results suggest that heat stress can suppress cap-dependent translation, at least in part through the accumulation of capped pre-tRNAs. We are aware that heat stress activates multiple translational regulatory pathways, including phosphorylation of eIF2α, changes in the availability of translation initiation factors, and phase separation–mediated mechanisms[61–66]. To address this limitation, we employed the tetO$_7$-*POP4* strain, which allows accumulation of capped pre-tRNAs without triggering other heat-

stress responses, and demonstrated that this accumulation represses the cap-dependent translation. Upon Dox treatment, the Rluc/Fluc ratio decreased to 20%, whereas no significant change was observed for the WT strain (Fig. 6h). Given that 5′ pre-tRFs are produced and capped upon heat stress (Fig. 1b–d), we asked whether the capped pre-tRFs have the ability to repress translation. To address this question, we performed the same dual-luciferase assay in an *rny1*Δ mutant in the $tetO_7$-*POP4* background. In the absence of *rny1*, the Rluc/Fluc ratio decreased to 11% (Fig. 6h), which is comparable to the reduction observed in the $tetO_7$-*POP4* strain (approximately 20% of control). These results indicate that the repression of cap-dependent translation observed in the $tetO_7$-*POP4* strain is primarily attributable to the capped pre-tRNAs, with minimal contribution from 5′ pre-tRFs.

Discussion

In this study, we employed CaSh-seq and found that pre-tRNA capping occurs in nearly all pre-tRNAs, enabling us to precisely map TSSs and TTSs of all tRNA genes in *S. cerevisiae*. Moreover, we discovered that many tRNA genes possess multiple TSSs. This finding is significant for tRNA biology for several reasons. First, the precise mapping of TSSs and TTSs enhances our understanding of RNAPIII transcriptional regulation, potentially yielding insights into how tRNA gene expression is regulated in response to cellular conditions and environmental stresses. Second, it may provide clues for identifying cis elements that regulate tRNA transcription, such as those influencing TSS selection and TTS readthrough, in addition to the essential transcriptional elements, including the internal promoter A and B boxes, upstream TATA elements that modulate transcription efficiency, and the oligo-T terminator sequence[16,17]. Third, this dataset provides accurate sequences of pri-tRNAs, establishing a foundation for detailed analyses of tRNA processing mechanisms. Indeed, in this study, the precise identification of 5′ leader and 3′ trailer sequences enabled high-resolution analysis of pre-tRNA secondary structures. Lastly, dynamic alteration of TSSs and TTSs under stress conditions could reveal adaptive mechanisms regulating tRNA production in response to environmental changes. Indeed, we confirmed alteration of TSS usage and extension of 3′ trailer sequences under heat stress conditions (Fig. 3e, f and Supplementary Fig. 7b).

The CaSh-seq method established in this study is also applicable for investigating the conservation and species-specificity of tRNA transcription and regulatory mechanisms in other eukaryotes, including humans and other mammals. In higher eukaryotes, regulation of 5′ capping of pre-tRNAs is more complex than in yeast, due to greater diversity of cap-binding proteins, decapping enzymes, and recapping systems[67–71].

Although nearly all pre-tRNAs are 5′ capped, the capping frequency varies significantly depending on the tRNA species (Fig. 4b, c and Supplementary Fig. 11). We demonstrated that pre-tRNAs with flexible 5′ leaders preferentially undergo 5′ capping (Fig. 5a, b). Interestingly, during heat stress, the cap score increased overall, and pre-tRNAs with reduced steady-state levels under heat stress conditions exhibited high cap scores (Fig. 4b, f and Supplementary Fig. 11a). These findings suggest that the terminal structures of pre-tRNAs may function as “RNA thermo-sensors” regulating cap modification efficiency.

Pre-tRNAs with flexible 5′ leaders are more susceptible to degradation by 5′ exonucleases Xrn1p and Rat1p[19], presumably under heat stress conditions. However, preferential capping of these pre-tRNAs is supposed to protect them from 5′ exonucleolytic degradation (Fig. 4f). Under environmental stress, tRNA processing is inhibited[1,72], temporarily halting mature tRNA production to regulate protein synthesis and reduce energy consumption. In this situation, accumulated pre-tRNAs are retained, and once growth conditions improve, they are rapidly processed to replenish the mature tRNA pool. Pre-tRNA capping plays a role in protecting accumulated pre-tRNAs from degradation.

Additionally, the terminal structures of pre-tRNAs likely play broader roles in determining tRNA fate. For example, two isoforms of pre-tW(CCA), which differ only in their 5′ leader and 3′ trailer sequences (Supplementary Data 5), follow distinct maturation pathways and have differential impacts on cell viability[73,74]. In the present study, we also observed significant differences in capping efficiency between these isoforms (Fig. 1b, c and Supplementary Data 8). These findings support the notion that the terminal structures of pre-tRNA act as regulatory elements controlling tRNA fate.

In *S. cerevisiae*, under oxidative stress conditions and during the stationary phase, Rny1p cleaves the anticodon loop of mature tRNAs, generating tRNA halves[47]. Using CaSh-seq, we detected a large number of capped 5′ pre-tRFs, which are generated by Rny1p (Figs. 1d, 4a, Supplementary Fig. 9). Furthermore, capped 5′ pre-tRFs were significantly accumulated under heat stress conditions (Figs. 1b–d, 4a, d and Supplementary Fig. 13a). Notably, 5′ pre-tRFs that decreased to steady-state levels under heat stress conditions exhibited high cap scores (Fig. 4g). Similar to capped pre-tRNAs, capped 5′ pre-tRFs might have some function to regulate protein synthesis. However, we had no evidence that the capped pre-tRFs repress cap-dependent translation (Fig. 6h). Considering that tRFs play pleiotropic roles in cellular processes, further studies are necessary to explore other physiological functions of capped 5′ pre-tRFs in various biological contexts.

Multiple mechanisms suppress cap-dependent translation in *S. cerevisiae* under heat stress conditions. They include phosphorylation of eIF2, activation of eIF4E-binding protein (4E-BP) Eap1p via the TORC1 pathway, and sequestration of untranslated mRNPs into heat-stress granule[61–66] (Fig. 7). Recent studies showed that a reduction or loss of eIF4E leads to various effects, including metabolic activation of aromatic amino acids through expression of *ARO9* transaminase and *ARO10* decarboxylase, promotion of the translation of *GCN4*, and suppression of the translation of *PCL5* (Pho85 cyclin 5), a negative regulator of *GCN4*[75,76]. Moreover, in mammalian cells, decreased availability of eIF4E preferentially reduces the translation of mRNAs bearing 5′-terminal oligopyrimidine (5′-TOP) sequences through activation of 4E-BPs such as 4E-BP1[77,78]. Various organisms produce 4E-BPs to regulate translation under different stress conditions[79,80], highlighting a universal mechanism for controlling cap-dependent translation across eukaryotes.

Under heat stress conditions, the terminal secondary structures of pre-tRNAs loosen, allowing the capping enzyme to add methyl-G caps to their flexible 5′ leaders (Fig. 7). Capped pre-tRNAs are exported to the cytoplasm where they sequester eIF4E, thereby inhibiting cap-dependent translation (Fig. 7). Supporting this hypothesis, experimental results indicate that eIF4E preferentially interacts with Pre 3 species generated in the cytoplasm, rather than with Pre 1 species primarily localized to the nucleus (Figs. 1a, 6b). Sequestration of eIF4E not only suppresses cap-dependent translation but also promotes mRNA localization to P-bodies or stress granules, potentially accelerating mRNA degradation (Fig. 7). Overall, capped pre-tRNAs may act as mRNA decoys that contribute to the suppression of cap-dependent translation under heat stress. Importantly, this effect is not expected to selectively repress specific stress-responsive mRNAs. Rather, pre-tRNA capping likely contributes to a global and transient reduction in eIF4E availability, acting in concert with other established translational control mechanisms during heat stress[61–66,81]. However, definitive demonstration that pre-tRNA capping alone can inhibit cap-dependent translation under heat stress conditions will require selective manipulation of the capping reaction, which remains technically challenging and is left for future work.

Pre-tRNA capping may also influence tRNA maturation through interactions with cap-binding proteins, eIF4E and Cbc2p (Fig. 7), potentially interfering with maturation by tethering pre-tRNAs and preventing their interaction with processing enzymes. Importantly, the preferential reduction of uncapped pre-tRNAs under heat stress does

not exclude the possibility that uncapped pre-tRNAs are more rapidly processed into mature tRNAs, rather than being capped. Dissecting the contribution of pre-tRNA capping to pre-tRNA stability and to the modulation of their maturation will require further investigation.

Finally, we considered the possibility that capped pre-tRNAs may be translated. We showed that capped pre-tRNAs interact with eIF4E and inhibit cap-dependent translation. If pre-tRNAs contain open reading frames (ORFs) encoding short peptides, it is conceivable that capped pre-tRNAs, through interaction with eIF4E, could be recruited into the translation initiation complex and undergo translation. For this to occur, the tertiary structure of pre-tRNAs would need to be unwound to allow the start codon to be recognized by the 48S pre-initiation complex (PIC)[58,82]. In general, strong secondary structures in the 5′ untranslated region (UTR) impair translation efficiency[83–85]. However, RNA helicases such as eIF4A and Ded1p can unwind these structures, enabling the 43S complex to scan for the start codon[58,82]. Efficient initiation also requires appropriate positioning of the AUG codon and Kozak sequence relative to the 5′ cap[58,82]. Structural analyses of the human 48S PIC suggest that a minimum distance of ~40 nucleotides between the 5′ end and the ribosomal P-site is required for initiation[86]. Notably, the average length of 5′ UTRs in yeast mRNAs is 53 nucleotides[82], but mRNAs with shorter 5′ UTRs can still be translated in *S. cerevisiae*[87], with even a 7-nucleotide 5′ UTR supporting translation at 50% of the optimal level[88]. Nevertheless, capped pre-tRNAs lack a poly(A) tail, and their stable structures and extensive post-transcriptional modifications may limit their translational competence. To investigate this possibility, we searched for potential ORFs within pre-tRNAs, and identified 288 AUG codons across pri- and spliced pre-tRNAs derived from 271 tRNA genes, distributed across various regions: 224 in exons, 50 in 5′ leaders, 10 in the intron of tP(UUG), and four in 3′ trailers (Supplementary Data 5). Notably, two-thirds of AUGs are located in 5′ regions. Interestingly, exon-located AUGs frequently occur in or near single-stranded regions such as the D-loop, anticodon loop, and variable region (Supplementary Data 5). However, these regions are heavily modified post-transcriptionally, which would likely hinder translation initiation by blocking recognition by initiator tRNAs. Therefore, under conditions of hypomodification or structural destabilization (e.g., heat stress), capped pre-tRNAs may become more susceptible to translation. To test this hypothesis, it will be important to examine the physical association of pre-tRNAs with the eIF4F complex and assess their presence in ribosomal fractions. In addition, ribosome profiling could be used to determine translation footprints derived from pre-tRNAs, providing further insights into their potential translatability.

Methods

Yeast strains, media, and growth conditions

The *S. cerevisiae* WT strain (BY4742: MATα; *his3Δ1*; *leu2Δ0*; *ura3Δ0*) and the *rny1*Δ strain (*rny1::KanMX4* in the BY4742 background) were obtained from EUROSCARF. The tetO$_7$-*POP4* strain was obtained from Horizon Discovery. To construct *rny1*Δ in the tetO$_7$-*POP4* background, *rny1* gene was replaced with *HIS3* marker by homologous recombination, as described in our previous report[19]. Recombinants that grew on SC medium without histidine were isolated. Deletion of the gene was verified by genomic PCR.

Yeast cells were grown in YPD medium (2% peptone, 1% yeast extract, 2% glucose). For plasmid maintenance, cells were cultured in SC-Leu medium (0.67% yeast nitrogen base without amino acids, 0.062% amino acid drop-out mix, 2% glucose, and 20 μg/mL of appropriate amino acids). For heat stress treatment, stationary-phase WT cells were inoculated into 50 mL YPD medium at an initial A_{600} of 0.2, cultured at 30 °C with shaking for 5 h, then subjected to heat stress at 34 °C, 37 °C, or 40 °C for 1–5 h. For CaSh-seq, WT cells were pre-cultured overnight in 50 mL YPD medium, then inoculated into fresh 50 mL YPD at A_{600} = 0.2 and cultured at 30 °C with shaking for 5 h, followed by heat stress at 37 °C for 3.5 h. The tetO$_7$-*POP4* strain was also pre-cultured overnight in 50 mL YPD, then inoculated into 50 mL YPD containing 20 μg/mL doxycycline (Dox) at A_{600} = 0.2, and incubated at 30 °C with shaking for either 4 or 7 h. Cells were harvested by centrifugation at 4,800 × *g* for 5 min at 4 °C, washed once with water, and centrifuged again under the same conditions. Strains and plasmids used in this study are listed in Supplementary Data 10. Sets of primers used for gene manipulation and PCR are listed in Supplementary Data 11.

Plasmid construction

The *eIF4E (CDC33)* and *CBC2* genes were amplified by PCR from genomic DNA of the BY4742 strain using primers containing a *Sal*I restriction enzyme site in the forward primer and a *Sac*I site along with a 3×FLAG tag in the reverse primer (Supplementary Data 11). The resulting PCR products and the pAD4 vector (bearing the *LEU2* selection marker) were digested with *Sal*I and *Sac*I, and ligated to generate FLAG-tagged expression constructs.

The pDual-Luc plasmid for in vivo dual luciferase assay was constructed by ligating two DNA fragments. The backbone was amplified by PCR from the plasmid pGADT7-ADH700-yeCherry-p150-yeGFP-DHFR (purchased from Addgene, this plasmid was a gift from Thomas Wandless, #24378; http://n2t.net/addgene:24378; RRID: Addgene_24378)[89]. The insert encoding the dual luciferase reporter was amplified from psiCHECK2-Eef2TOP-RLCP-HCVIRES-FL, provided by the Shintaro Iwasaki Lab[90]. The hCL/hPEST (CP) degradation signal[91] was inserted at the N-terminus of Fluc. The HCV-IRES sequence was replaced by CrPV-IRES to enhance IRES-dependent translation efficiency in *S. cerevisiae*[92]. All manipulation of plasmid constructs was performed by the SLiCE method[93]. All primers used in this study are listed in Supplementary Data 11.

Preparation of total RNA and small RNA from yeast cells

Total RNA was extracted from yeast cells using a modified version of a previously described method[94]. Cell pellets were resuspended in 10 volumes of RNA extraction buffer comprising 50 mM sodium acetate pH 5.3, and 10 mM ethylenediaminetetraacetic acid (EDTA), mixed with an equal volume of water-saturated phenol, and shaken either for 2 h at 37 °C or for 1 h at 65 °C. Samples were then centrifuged at 10,000 × *g* for 30 min at 4 °C. The aqueous phase was collected, mixed with an equal volume of chloroform, and centrifuged again at 10,000 × *g* for 30 min at 4 °C. The resulting supernatant was precipitated with isopropanol to obtain total RNA.

To prepare the small RNA fractions, total RNA was subjected to anion-exchange chromatography using DEAE-Sepharose Fast Flow resin (Cytiva) under gravitational flow. Buffer A comprising 20 mM HEPES-KOH pH 7.5, 250 mM NaCl, and 2 mM dithiothreitol (DTT) was used for column equilibration, RNA binding, and washing. Buffer B (20 mM HEPES-KOH pH 7.5, 1 M NaCl, 2 mM DTT) was used for elution of small RNAs. Eluted RNA was recovered by ethanol precipitation.

Immunoprecipitation of RNA bearing methylguanosine caps

A total of 200 μg of either total RNA or small RNA fractions was resuspended in 300 μL of cap-binding buffer (25 mM Tris-HCl pH 7.5, 200 mM NaCl, 5 mM EDTA, 0.2% Tween-20, 0.5 mM DTT, 0.1U/μL SUPERase•In) from Thermo Fisher Scientific. RNA was mixed with a 20 μL bed volume of anti-2,2,7-trimethylguanosine (TMG) antibody-conjugated agarose beads (Clone K121, catalog no. NA02A, Merck), pre-equilibrated in cap-binding buffer, and incubated with rotation for 2 h at 4 °C. Beads were then washed five times with 500 μL of cap-binding buffer and bound RNAs were extracted using TRIzol LS Reagent (Thermo Fisher Scientific) following the manufacturer's protocol.

Northern blotting

A total of 200 ng of RNA was resolved by electrophoresis on a 10% denaturing polyacrylamide gel and transferred to a Hybond N^+ membrane (Cytiva) by electroblotting for 1 h at 1.5 mA/cm². The membrane was dried and UV crosslinked (254 nm, 120 mJ/cm², CL-1000, UVP) twice to immobilize RNA. Pre-hybridization was performed in 7 mL of homemade hybridization buffer comprising 500 mM sodium phosphate buffer pH 7.4, 1 mM EDTA, 7.5% sodium dodecyl sulfate (SDS), 5% polyethylene glycol (PEG) 6000, 0.5% casein, and 0.1% NaN_3 at 53 °C for 1 h. Hybridization was then carried out overnight at 53 °C using 2 pmol of 5′-^{32}P-labeled DNA probes. Probe sequences are listed in Supplementary Data 11. After hybridization, the membrane was washed five times with 2× SSC (300 mM NaCl, 30 mM sodium citrate), dried, and exposed to an imaging plate (FUJIX). Radioactive signals were visualized using an FLA-7000 imaging analyzer (Fujifilm) and analyzed with Multi Gauge software (Fujifilm).

Northwestern blotting

The $tetO_7$-*POP4* strain was pre-cultured overnight in YPD medium, then inoculated into fresh YPD containing 20 μg/mL Dox at an initial A_{600} of 0.2, and cultured at 30 °C with shaking for 0, 1, 2, 4, 6, or 8 h. Total RNA was extracted as described above. One microgram of RNA was resolved by electrophoresis on a 10% denaturing polyacrylamide gel, transferred to a Hybond N^+ membrane (Cytiva), UV crosslinked using the same protocol as described for northern blotting, then blocked with 20% EzBlock Chemi (ATTO) for 1 h at room temperature. The membrane was incubated overnight at 4 °C with an antibody against the TMG cap (mouse monoclonal antibody, clone K121, catalog no. MABE302, Merck) as primary antibody at a dilution of 1:2000, followed by three washes with 1× TBST buffer. The membrane was then incubated for 1 h at room temperature with a horseradish peroxidase (HRP)-conjugated mouse IgG (polyclonal, catalog no. HAF007, R&D Systems) as secondary antibody at a dilution of 1:1000, followed by four additional washes with 1× TBST. Capped RNA signals were detected using Pierce ECL Plus Western Blotting Substrate (Thermo Fisher Scientific) and visualized with an ImageQuant LAS 4000 mini system (Cytiva).

Isolation of pre-tRNA

Pre-tRNA isolation from total RNA of $tetO_7$-*POP4* strain was performed by reciprocal circulating chromatography, according to our previous study[19,95]. The sequence of oligo DNA probe is shown in Supplementary Data 11.

LC/MS analysis

RNA fragment analysis was performed as previously described[96,97] with slight modifications. Briefly, 30 ng (~900 fmol) of RNA was digested in 10 μL of reaction buffer containing 20 mM ammonium acetate (NH_4OAc, pH 7.7) and 10 ng RNase A (Thermo Fisher Scientific), and incubated at 37 °C for 30 min. An equal volume of 0.1 M triethylammonium acetate (TEAA, pH 7.0) was then added to the digest for LC/MS analysis. The RNA digest was desalted using a trap column and separated by liquid chromatography on a HiQ sil C18W-3 capillary column (C18, 3 μm, 120 Å pore size, 0.15 mm ID × 50 mm, KYA Technologies). The mobile phase consisted of solvent A (0.4 M hexafluoroisopropanol [HFIP], pH 7.0) and solvent B (50% methanol), and separation was performed with a linear gradient from 0% to 80% B over 40 min at a flow rate of 500 nL/min. The eluent was introduced directly into the electrospray ionization (ESI) source of LTQ Orbitrap XL (Thermo Fisher Scientific) or Q Exactive Hybrid Quadrupole-Orbitrap mass spectrometer (Thermo Fisher Scientific). Ionization was performed using a conductive spray tip attached to the capillary column, and ions were detected in negative polarity mode across an *m/z* range of 600–2,000 during chromatographic separation.

Construction of a cDNA library for CaSh-seq

Small RNA (400 ng), prepared as described above, was 3′-dephosphorylated at 37 °C for 1 h in 100 μL of T4 PNK Reaction Buffer (70 mM Tris-HCl pH 7.5, 10 mM $MgCl_2$, 5 mM DTT, 0.1 U/μL SUPERase•In, 0.2 U/μL T4 polynucleotide kinase; NEB). The reaction mixture was then purified by phenol:chloroform:isoamyl alcohol (PCI) extraction, followed by chloroform extraction and ethanol precipitation. A total of 200 ng of 3′-dephosphorylated RNA was ligated to a 3′ adapter at 25 °C for 16 h in a mixture containing 1× T4 RNA Ligase Reaction Buffer (NEB), 1 μM Universal miRNA Cloning Linker (NEB), 25% PEG 8000, 2 U/μL SUPERase•In, and 10 U/μL T4 RNA Ligase 2 (truncated KQ, NEB). The ligation product was purified by PCI extraction, chloroform extraction, and ethanol precipitation. To remove excess 3′ adapters, ligation products were resolved by 10% denaturing polyacrylamide gel electrophoresis (PAGE), excised, gel-purified, then dissolved in 11.2 μL of nuclease-free water. For reverse transcription (RT), 0.8 μL of RT primer (3.75 μM) was added to the RNA sample, denatured at 80 °C for 5 min, and cooled to room temperature. RT was carried out by adding 8 μL of TGIRT Reaction Buffer (50 mM Tris-HCl pH 7.5, 12.5 mM $MgCl_2$, 1,125 mM NaCl, 2.5 mM dNTPs, 12.5 mM DTT, 2.5U/μL SUPERase•In, 1 μL TGIRT-III; InGex) to the RNA-primer mixture, followed by incubation at 57 °C for 2 h. The reaction was quenched by adding 1.1 μL of 2 M NaOH and incubating at 95 °C for 5 min. First-strand cDNA was then purified by ethanol precipitation and gel-purified using 6% denaturing PAGE. The purified cDNA was circularized at 60 °C for 16 h in a reaction containing 1× CircLigase Reaction Buffer, 2.5 mM $MnCl_2$, 50 μM ATP, and 5 U/μL CircLigase II (Lucigen). The reaction was heat-inactivated at 80 °C for 10 min and purified sequentially by PCI extraction, chloroform extraction, and ethanol precipitation. One-quarter of the circularized cDNA was used as a template for PCR amplification (14 cycles) in a reaction mixture containing 1× Phusion GC Buffer, 0.2 mM dNTPs, 0.5 μM forward and reverse PCR primers (Supplementary Data 11), 3% dimethyl sulfoxide (DMSO), and 20 U/mL Phusion polymerase (NEB). PCR products were purified using AMPure XP beads (Beckman Colter), followed by gel purification by 6% native PAGE, and a second AMPure XP purification. The final cDNA libraries were sequenced in 150 base pair (bp) paired-end mode on a HiSeq-4000 platform (Illumina).

CaSh-seq data processing and mapping

Raw sequencing reads were processed using fastp v0.20.0 (https://github.com/OpenGene/fastp) for unique molecular identifier (UMI) extraction, adapter trimming, and low-quality read filtering. The 15-nt UMI sequence located at the beginning of Read 1 was extracted and appended to the read name using the --umi option in fastp. The minimum read length after trimming was set to 15 nt, and the quality threshold was set to Q15. PCR duplicates were removed based on the UMI sequences. Trimmed and deduplicated reads were mapped to the *S. cerevisiae* S288C reference genome (version R64-1-1, obtained from EnsemblFungi) using STAR v2.7.3a (https://github.com/alexdobin/STAR) with the following options:

--outMultimapperOrder Random
--alignIntronMax 1
--scoreGapNoncan 0
--scoreGapGCAG 0
--scoreGapATAC 0
--outSJfilterOverhangMin 8 8 8 8
--outFilterMismatchNmax 5
--outFilterMultimapNmax 20

Statistics for read trimming and mapping are summarized in Supplementary Data 1. Gene-level read counts across all *S. cerevisiae* genes in the CaSh-seq datasets are provided in Supplementary Data 2.

Aligned reads in BAM format were processed using custom Python scripts implemented with the Biopython and pysam libraries. To reduce bias associated with multi-mapped reads, BAM files were

first sorted by read name to group all alignments derived from the same read. One alignment per read was then randomly selected from all candidate alignments, regardless of the NH value, so that each candidate locus had an equal probability of being retained. Based on these selected alignments, a new BAM file containing only one retained alignment per read was generated. Thus, each read contributed only once to downstream analyses. The resulting BAM files were subsequently sorted by genomic coordinates and indexed for further analysis. Visualizations were generated in R v4.2.1.

Determination of TSSs and TTSs

To determine TSSs of tRNA genes from Illumina reads, only Read 1 was analyzed. Read 2 was excluded because the UMI sequences had not been removed, resulting in misalignment and reduced accuracy in TSS determination. RNAPIII typically initiates transcription at a purine (A or G) located within a pyrimidine-purine (Py-Pu) motif upstream of the 5′ processing site (5′PS). Therefore, TSS candidates were identified based on the following criteria: (1) The purine is located at the 5′ end of the read. (2) The purine is immediately downstream of a pyrimidine in the genomic sequence. (3) The purine accounts for more than 25% of all reads that satisfy conditions (1) and (2), with a coefficient of variation below 20% across three biological replicates. Reads that did not meet these criteria or contained soft-clipped regions at the 5′ end were excluded from further analysis. For each tRNA gene, the relative proportion of each TSS candidate was calculated as a fraction of the total reads satisfying the TSS selection criteria. TTSs were defined based on the presence of five or more consecutive thymidine (T) residues located within 50 nucleotides downstream of the 3′ processing site (3′ PS). The canonical TTS was selected as the position showing the largest decrease in read coverage in the Input sample of the tetO_7-*POP4* strain treated with Dox for 4 h, as described in previous study[17].

Classification of tRNA gene-mapped reads

Reads mapped to tRNA genes were classified into distinct precursors or tRFs according to their maturation or processing states using the "Tag code" system, an index that reflects the processing pattern of each tRNA, based on the presence or absence of specific residues located at defined regions of tRNA genes including exon, intron, 5′ leader, and 3′ trailer sequences (Supplementary Fig. 8). Through this procedure, multimapping reads that correspond to mature tRNAs are removed from the analysis.

Cap score calculation

Cap score was calculated to evaluate the capping efficiency of pre-tRNAs or 5′ pre-tRFs, and is defined by the following equation (Supplementary Fig. 10a):

$$\text{Cap score} = \frac{\frac{\text{Read count of pre-tRNA or 5′ pre-tRF with 5′ leader in IP}}{\text{Read count of pre-tRNA or 5′ pre-tRF with 5′ leader in Input}}}{\frac{\text{Read count of U4 snRNA in IP}}{\text{Read count of U4 snRNA in Input}}} \quad (1)$$

For the calculation, read counts at the nucleotide located four bases upstream of the 5′PS (position −4) were used to quantify pre-tRNA- or 5′ pre-tRF-derived reads (Supplementary Fig. 10b). Genes with five or more reads mapped to the 5′ leader sequence in the Input sample were considered for analysis. U4 snRNA, presumed to be fully capped, was used as an internal reference for normalization. Bicistronic tRNA genes were excluded from cap score and related quantitative analyses because a single primary transcript contains two tRNA units that are separated by internal processing, making the definition of a single pre-tRNA unit ambiguous.

Base pairing probability

The base-pairing probability at the 5′ end of each pri-tRNA was calculated using CentroidFold[57]. For this analysis, the sequence corresponding to the acceptor stem along with the 5′ leader and 3′ trailer regions of each pri-tRNA was used. The basal ends of the acceptor stem were connected with a randomized 30-nt linker (N30) to facilitate folding prediction (Supplementary Fig. 15, Supplementary Data 9). For tRNA genes with multiple TSSs, if the predominant TSSs at 4 h and 7 h Dox-treated samples were identical, that TSS was used; otherwise, the TSS matching the predominant one in the WT Control sample was selected.

Purification of capped RNA bound to FLAG-tagged protein

FLAG-tagged expression constructs for *eIF4E* and *CBC2*, along with the empty pAD4 vector, were introduced into the tetO_7-*POP4* strain using the lithium acetate/single-stranded carrier DNA/PEG method[98]. Transformants were selected on SC-Leu plates. The tetO_7-*POP4* strains harboring pAD4 (empty vector), FLAG-tagged eIF4E, or FLAG-tagged Cbc2p were cultured overnight in 50 mL SC-Leu medium at 30 °C. Fully grown cells were inoculated into 200 mL SC-Leu medium containing 10 μg/mL Dox at an initial A_{600} of 0.1 and cultured at 30 °C for 10 h with shaking.

Cells were harvested by centrifugation at 4000 × *g* for 10 min at 4 °C, washed once with double-distilled water, centrifuged again, and resuspended in phosphate-buffered saline. Crosslinking was performed by treating cells with 0%, 0.005%, or 0.02% formaldehyde at room temperature for 10 min. The reaction was quenched by adding a one-tenth volume of 2 M glycine (final concentration ~0.2 M) and incubating for 10 min at room temperature. Cells were washed with ice-cold TBS buffer then flash-frozen in liquid nitrogen. For crude lysate preparation, frozen cells were ground in liquid nitrogen using a mortar and pestle and resuspended in ~20 mL ice-cold lysis buffer comprising 50 mM HEPES-KOH pH 7.4, 200 mM KCl, 10 mM $MgCl_2$, 7 mM 2-mercaptoethanol, 2 mM phenylmethylsulfonyl fluoride (PMSF), 16% glycerol, and protease inhibitor cocktail (Roche). The lysate was clarified by ultracentrifugation at 45,000 × *g* for 1 h and filtered through a 0.45 μm filter.

For immunoprecipitation, 4.5 mL of the clarified lysate was incubated with 400 μL of Anti-FLAG M2 agarose beads (clone M2, catalog no. A2220 Merck), pre-equilibrated in Binding/Washing buffer (50 mM HEPES-KOH pH 7.4, 500 mM KCl, 10 mM $MgCl_2$, 7 mM 2-mercaptoethanol, 2 mM PMSF, 0.5% Triton X-100, cOmplete Protease Inhibitor Cocktail; Merck) at 4 °C for 2 h. Beads were washed four times with 4 mL of the same buffer, followed by one wash with 4 mL TE/100 mM NaCl buffer (10 mM Tris-HCl pH 8.0, 1 mM EDTA, 100 mM NaCl, 7 mM 2-mercaptoethanol, 2 mM PMSF, cOmplete Protease Inhibitor Cocktail). Bound proteins and associated RNAs were eluted by incubation with 400 μL of FLAG extraction buffer (50 mM HEPES-KOH pH 7.4, 500 mM KCl, 10 mM $MgCl_2$, 7 mM 2-mercaptoethanol, 2 mM PMSF, 16% glycerol, 200 μg/mL FLAG peptide) at 4 °C for 1 h. The eluate was then treated with NaCl (final concentration 200 mM) and SUPERase•In (0.2 U/μL), followed by incubation at 65 °C for 1 h to reverse crosslinking.

Co-eluted RNAs associated with FLAG-tagged proteins were extracted using TRIzol LS Reagent (Thermo Fisher Scientific) following the manufacturer's protocol. Successful FLAG pulldown was confirmed by western blotting using an anti-DDDDK-tag HRP-conjugated antibody (polyclonal, catalog no. PM020-7, MBL International Corporation) at a dilution of 1:5000. Proteins were detected using Pierce ECL Plus Western Blotting Substrate (Thermo Fisher Scientific) and visualized with an ImageQuant LAS 4000 mini system (Cytiva).

In vitro translation assay

Capped pre-tRNAs were prepared from 250 μg of total RNA extracted from the tetO_7-*POP4* strain treated with Dox for 7 h, as described above, and purified using 10% denaturing PAGE. Chemical decapping of the capped pre-tRNAs was performed via periodate oxidation followed by β-elimination as described previously[97] with slight modifications. Specifically, 2 μg of the capped pre-tRNA was dissolved in

100 µL of 10 mM sodium periodate ($NaIO_4$) and incubated on ice for 1 h in the dark to oxidize the 2′,3′-cis-diol of the ribose in the cap structure, yielding a 2′,3′-dialdehyde. RNA was purified by ethanol precipitation, dissolved in 1 M lysine-HCl (pH 8.5), and incubated at 45 °C for 90 min to induce β-elimination. The resulting decapped RNA was purified again by ethanol precipitation.

A Wheat Germ Extract Translation Kit (TLS4050, NUProtein) was used to perform in vitro translation. Capped and decapped pre-tRNAs were resuspended in 10 µL of reaction buffer containing 10 mM amino acid mix, 10% wheat germ extract, and 100 ng of 5′ capped Nluc mRNA, which was synthesized in vitro using a HiScribe T7 High Yield RNA Synthesis Kit (NEB). Final concentrations of pre-tRNA in the reaction were adjusted to 0, 0.262, 2.62, 26.2, 131, and 262 nM. The reaction mixtures were incubated at 16 °C for 10 min.

A Rabbit Reticulocyte Lysate (RRL), Nuclease-treated translation system (L4960, Promega) was used to perform in vitro translation. Capped and decapped pre-tRNAs were resuspended in 5 µL of reaction buffer containing 70% RRL and 2% amino acid mixture prepared as a 1:1 combination of Minus Leucine and Minus Methionine mixes, together with 50 ng of either 5′ capped Nluc mRNA or CrPV-IRES Nluc mRNA, both of which were synthesized in vitro using a HiScribe T7 High Yield RNA Synthesis Kit (NEB). Final concentrations of pre-tRNA in the reaction were adjusted to 0, 26.2, 131, and 262 nM. The reactions were incubated at 30 °C for 10 min.

Luminescence from Nluc was measured using a Nano-Glo Luciferase Assay System (Promega) on a GloMax luminometer (Promega).

In vivo dual luciferase assay

WT, $tetO_7$-*POP4*, and $tetO_7$-*POP4 rny1*Δ strains carrying the pDual-Luc plasmid were pre-cultured overnight in SC-Leu medium, then inoculated into fresh 2 mL YPD medium with or without 20 µg/mL Dox at an initial A_{600} of 0.2 and cultured at 30 °C for 7 h with shaking. For heat-stress experiments, WT strain with the pDual-Luc plasmid was inoculated into fresh 2 mL SC-Leu medium at an initial A_{600} of 0.2 and cultured at 30 °C for 5 h. Cells were then shifted to 37 °C and further cultured for 3.5 h. Control samples were cultured in parallel at 30 °C for a total of 8.5 h. Yeast cells were harvested and lysed using a ShakeMaster NEO system (Bio Medical Science). The cell pellet was resuspended in lysis buffer (50 mM HEPES-KOH pH 7.4, 200 mM KCl, 20 mM $MgCl_2$, 7 mM 2-mercaptoethanol, 2 mM PMSF, protease inhibitor cocktail; Roche), and 20 U/mL SUPERase•In. Lysates were centrifuged at 4 °C for 5 min at 4800 × *g*, and supernatants were filtered through Millex-HV 0.45µm polyvinylidene difluoride (PVDF) filters (Merck). Luciferase activity was measured using a Dual-Glo Luciferase Assay System (Promega). For Fluc measurement, 5 µL of cell lysate was mixed with 50 µL of LARII reagent in a 96-well plate, and luminescence was recorded using a GloMax luminometer (Promega). As a negative control, 5 µL of lysis buffer without lysate was used to measure background signal. Following Fluc measurement, 50 µL of Stop & Glo reagent was added to quench Fluc activity. Rluc substrate was then added, and luminescence intensity was measured using the same instrument.

Reporting summary

Further information on research design is available in the Nature Portfolio Reporting Summary linked to this article.

Data availability

Source data are provided with this paper. The CaSh-seq data generated in this study have been deposited in the NCBI Sequence Read Archive (SRA) under accession number PRJNA1070052. Source data are provided with this paper.

Code availability

All original code is available from a public GitHub repository https://github.com/ITKKC/cashseqcalc.

References

1. Phizicky, E. M. & Hopper, A. K. The life and times of a tRNA. *RNA* **29**, 898–957 (2023).
2. Suzuki, T. The expanding world of tRNA modifications and their disease relevance. *Nat. Rev. Mol. Cell Biol.* **22**, 375–392 (2021).
3. Hanson, G. & Coller, J. Codon optimality, bias and usage in translation and mRNA decay. *Nat. Rev. Mol. Cell Biol.* **19**, 20–30 (2018).
4. Presnyak, V. et al. Codon optimality is a major determinant of mRNA stability. *Cell* **160**, 1111–1124 (2015).
5. Nedialkova, D. D. & Leidel, S. A. Optimization of codon translation rates via tRNA modifications maintains proteome integrity. *Cell* **161**, 1606–1618 (2015).
6. Zhao, X. et al. Glycosylated queuosines in tRNAs optimize translational rate and post-embryonic growth. *Cell* **186**, 5517–5535 e5524 (2023).
7. Pechmann, S. & Frydman, J. Evolutionary conservation of codon optimality reveals hidden signatures of cotranslational folding. *Nat. Struct. Mol. Biol.* **20**, 237–243 (2013).
8. Orellana, E. A., Siegal, E. & Gregory, R. I. tRNA dysregulation and disease. *Nat. Rev. Genet* **23**, 651–664 (2022).
9. Ohira, T. & Suzuki, T. Transfer RNA modifications and cellular thermotolerance. *Mol. Cell* **84**, 94–106 (2024).
10. Foretek, D., Wu, J., Hopper, A. K. & Boguta, M. Control of Saccharomyces cerevisiae pre-tRNA processing by environmental conditions. *RNA* **22**, 339–349 (2016).
11. Gudipati, R. K. et al. Extensive degradation of RNA precursors by the exosome in wild-type cells. *Mol. Cell* **48**, 409–421 (2012).
12. Schneider, C., Kudla, G., Wlotzka, W., Tuck, A. & Tollervey, D. Transcriptome-wide analysis of exosome targets. *Mol. cell* **48**, 422–433 (2012).
13. Alexandrov, A. et al. Rapid tRNA decay can result from lack of nonessential modifications. *Mol. cell* **21**, 87–96 (2006).
14. Payea, M. J., Hauke, A. C., De Zoysa, T. & Phizicky, E. M. Mutations in the anticodon stem of tRNA cause accumulation and Met22-dependent decay of pre-tRNA in yeast. *RNA* **26**, 29–43 (2020).
15. Chan, P. P. & Lowe, T. M. GtRNAdb 2.0: an expanded database of transfer RNA genes identified in complete and draft genomes. *Nucleic Acids Res.* **44**, D184–D189 (2016).
16. Arimbasseri, A. G. & Maraia, R. J. RNA polymerase III advances: structural and tRNA functional views. *Trends Biochem. Sci.* **41**, 546–559 (2016).
17. Turowski, T. W. et al. Global analysis of transcriptionally engaged yeast RNA polymerase III reveals extended tRNA transcripts. *Genome Res.* **26**, 933–944 (2016).
18. Bachman, N., Eby, Y. & Boeke, J. D. Local definition of Ty1 target preference by long terminal repeats and clustered tRNA genes. *Genome Res.* **14**, 1232–1247 (2004).
19. Ohira, T. & Suzuki, T. Precursors of tRNAs are stabilized by methylguanosine cap structures. *Nat. Chem. Biol.* **12**, 648–655 (2016).
20. Xiao, S., Houser-Scott, F. & Engelke, D. R. Eukaryotic ribonuclease P: increased complexity to cope with the nuclear pre-tRNA pathway. *J. Cell. Physiol.* **187**, 11–20 (2001).
21. Skowronek, E., Grzechnik, P., Spath, B., Marchfelder, A. & Kufel, J. tRNA 3′ processing in yeast involves tRNase Z, Rex1, and Rrp6. *RNA* **20**, 115–130 (2014).
22. Kufel, J., Allmang, C., Verdone, L., Beggs, J. D. & Tollervey, D. LSM proteins are required for normal processing of pre-tRNAs and their efficient association with La-homologous protein Lhp1p. *Mol. Cell. Biol.* **22**, 5248–5256 (2002).
23. Betat, H., Rammelt, C. & Mörl, M. tRNA nucleotidyltransferases: ancient catalysts with an unusual mechanism of polymerization. *Cell. Mol. Life Sci. CMLS* **67**, 1447–1463 (2010).
24. Jackman, J. E., Gott, J. M. & Gray, M. W. Doing it in reverse: 3′-to-5′ polymerization by the Thg1 superfamily. *RNA* **18**, 886–899 (2012).

25. Chatterjee, K., Marshall, W. A. & Hopper, A. K. Three tRNA nuclear exporters in S. cerevisiae: parallel pathways, preferences, and precision. *Nucleic Acids Res.* **50**, 10140–10152 (2022).
26. Ohira, T. & Suzuki, T. Retrograde nuclear import of tRNA precursors is required for modified base biogenesis in yeast. *Proc. Natl. Acad. Sci. USA* **108**, 10502–10507 (2011).
27. Wan, Y. & Hopper, A. K. From powerhouse to processing plant: conserved roles of mitochondrial outer membrane proteins in tRNA splicing. *Genes Dev.* **32**, 1309–1314 (2018).
28. Yoshihisa, T., Ohshima, C., Yunoki-Esaki, K. & Endo, T. Cytoplasmic splicing of tRNA in Saccharomyces cerevisiae. *Genes Cells. Mol. Cell. Mech.* **12**, 285–297 (2007).
29. O'Connor, J. P. & Peebles, C. L. In vivo pre-tRNA processing in Saccharomyces cerevisiae. *Mol. Cell. Biol.* **11**, 425–439 (1991).
30. Kramer, E. B. & Hopper, A. K. Retrograde transfer RNA nuclear import provides a new level of tRNA quality control in Saccharomyces cerevisiae. *Proc. Natl. Acad. Sci. USA* **110**, 21042–21047 (2013).
31. Nostramo, R. T. et al. Free introns of tRNAs as complementarity-dependent regulators of gene expression. *Mol. cell* **85**, 726–741 e726 (2025).
32. Muthukumar, S., Li, C. T., Liu, R. J. & Bellodi, C. Roles and regulation of tRNA-derived small RNAs in animals. *Nat. Rev. Mol. Cell Biol.* **25**, 359–378 (2024).
33. Honda, S. et al. Sex hormone-dependent tRNA halves enhance cell proliferation in breast and prostate cancers. *Proc. Natl. Acad. Sci. USA* **112**, E3816–E3825 (2015).
34. Magee, R. & Rigoutsos, I. On the expanding roles of tRNA fragments in modulating cell behavior. *Nucleic Acids Res.* **48**, 9433–9448 (2020).
35. Kumar, P., Anaya, J., Mudunuri, S. B. & Dutta, A. Meta-analysis of tRNA derived RNA fragments reveals that they are evolutionarily conserved and associate with AGO proteins to recognize specific RNA targets. *BMC Biol.* **12**, 78 (2014).
36. Xie, Y. et al. Action mechanisms and research methods of tRNA-derived small RNAs. *Signal Transduct. Target Ther.* **5**, 109 (2020).
37. Yu, M. et al. tRNA-derived RNA fragments in cancer: current status and future perspectives. *J. Hematol. Oncol.* **13**, 121 (2020).
38. Weng, Q. et al. Extracellular vesicles-associated tRNA-derived fragments (tRFs): biogenesis, biological functions, and their role as potential biomarkers in human diseases. *J. Mol. Med.***100**, 679–695 (2022).
39. Furuichi, Y. Discovery of m(7)G-cap in eukaryotic mRNAs. *Proc. Jpn. Acad. Ser. B, Phys. Biol. Sci.* **91**, 394–409 (2015).
40. Topisirovic, I., Svitkin, Y. V., Sonenberg, N. & Shatkin, A. J. Cap and cap-binding proteins in the control of gene expression. *Wiley Interdiscip. Rev. RNA* **2**, 277–298 (2011).
41. Pelletier, J., Schmeing, T. M. & Sonenberg, N. The multifaceted eukaryotic cap structure. *Wiley Interdiscip. Rev. RNA* **12**, e1636 (2021).
42. Matera, A. G., Terns, R. M. & Terns, M. P. Non-coding RNAs: lessons from the small nuclear and small nucleolar RNAs. *Nat. Rev. Mol. cell Biol.* **8**, 209–220 (2007).
43. Rambout, X. & Maquat, L. E. The nuclear cap-binding complex as choreographer of gene transcription and pre-mRNA processing. *Genes Dev.* **34**, 1113–1127 (2020).
44. Galloway, A & Cowling, V. H. mRNA cap regulation in mammalian cell function and fate. *Biochimica et. Biophysica Acta Gene Regul. Mech.* **1862**, 270–279 (2019).
45. Leung, D. W. & Amarasinghe, G. K. When your cap matters: structural insights into self vs non-self recognition of 5′ RNA by immunomodulatory host proteins. *Curr. Opin. Struct. Biol.* **36**, 133–141 (2016).
46. Yamagami, R., Sieg, J. P., Assmann, S. M. & Bevilacqua, P. C. Genome-wide analysis of the in vivo tRNA structurome reveals RNA structural and modification dynamics under heat stress. *Proc. Natl. Acad. Sci. USA* **119**, e2201237119 (2022).
47. Thompson, D. M. & Parker, R. The RNase Rny1p cleaves tRNAs and promotes cell death during oxidative stress in Saccharomyces cerevisiae. *J. Cell Biol.* **185**, 43–50 (2009).
48. Jia, D. et al. Systematic identification of non-coding RNA 2,2,7-trimethylguanosine cap structures in Caenorhabditis elegans. *BMC Mol. Biol.* **8**, 86 (2007).
49. Xu, H., Yao, J., Wu, D. C. & Lambowitz, A. M. Improved TGIRT-seq methods for comprehensive transcriptome profiling with decreased adapter dimer formation and bias correction. *Sci. Rep.* **9**, 7953 (2019).
50. Hiley, S. L., Babak, T. & Hughes, T. R. Global analysis of yeast RNA processing identifies new targets of RNase III and uncovers a link between tRNA 5′ end processing and tRNA splicing. *Nucleic Acids Res.* **33**, 3048–3056 (2005).
51. Zheng, G. et al. Efficient and quantitative high-throughput tRNA sequencing. *Nat. Methods* **12**, 835–837 (2015).
52. Clark, W. C., Evans, M. E., Dominissini, D., Zheng, G. & Pan, T. tRNA base methylation identification and quantification via high-throughput sequencing. *RNA* **22**, 1771–1784 (2016).
53. Engelke, D. R., Gegenheimer, P. & Abelson, J. Nucleolytic processing of a tRNAArg-tRNAAsp dimeric precursor by a homologous component from Saccharomyces cerevisiae. *J. Biol. Chem.* **260**, 1271–1279 (1985).
54. Brachmann, C. B. et al. Designer deletion strains derived from Saccharomyces cerevisiae S288C: a useful set of strains and plasmids for PCR-mediated gene disruption and other applications. *Yeast* **14**, 115–132 (1998).
55. Asif-Laidin, A. et al. A small targeting domain in Ty1 integrase is sufficient to direct retrotransposon integration upstream of tRNA genes. *EMBO J.* **39**, e104337 (2020).
56. Zecherle, G. N., Whelen, S. & Hall, B. D. Purines are required at the 5′ ends of newly initiated RNAs for optimal RNA polymerase III gene expression. *Mol. Cell. Biol.* **16**, 5801–5810 (1996).
57. Sato, K., Hamada, M., Asai, K. & Mituyama, T. CENTROIDFOLD: a web server for RNA secondary structure prediction. *Nucleic Acids Res.* **37**, W277–W280 (2009).
58. Brito Querido, J., Díaz-López, I. & Ramakrishnan, V. The molecular basis of translation initiation and its regulation in eukaryotes. *Nat. Rev. Mol. Cell Biol.* **25**, 168–186 (2024).
59. Pestova, T. V., Lomakin, I. B. & Hellen, C. U. Position of the CrPV IRES on the 40S subunit and factor dependence of IRES/80S ribosome assembly. *EMBO Rep.* **5**, 906–913 (2004).
60. Jan, E. & Sarnow, P. Factorless ribosome assembly on the internal ribosome entry site of cricket paralysis virus. *J. Mol. Biol.* **324**, 889–902 (2002).
61. Muhlhofer, M. et al. The heat shock response in yeast maintains protein homeostasis by chaperoning and replenishing proteins. *Cell Rep.* **29**, 4593–4607 e4598 (2019).
62. Iserman, C. et al. Condensation of Ded1p promotes a translational switch from housekeeping to stress protein production. *Cell* **181**, 818–831 e819 (2020).
63. Takahara, T. & Maeda, T. Transient sequestration of TORC1 into stress granules during heat stress. *Mol. cell* **47**, 242–252 (2012).
64. Grousl, T. et al. Robust heat shock induces eIF2alpha-phosphorylation-independent assembly of stress granules containing eIF3 and 40S ribosomal subunits in budding yeast, Saccharomyces cerevisiae. *J. cell Sci.* **122**, 2078–2088 (2009).
65. Cherkasov, V. et al. Coordination of translational control and protein homeostasis during severe heat stress. *Curr. Biol.* **23**, 2452–2462 (2013).
66. Hinnebusch, A. G. eIF2alpha kinases provide a new solution to the puzzle of substrate specificity. *Nat. Struct. Mol. Biol.* **12**, 835–838 (2005).

67. Rehwinkel, J. & Gack, M. U. RIG-I-like receptors: their regulation and roles in RNA sensing. *Nat. Rev. Immunol.* **20**, 537–551 (2020).
68. Weiss, B. et al. eIF4E3 forms an active eIF4F complex during stresses (eIF4FS) targeting mTOR and re-programs the translatome. *Nucleic Acids Res.* **49**, 5159–5176 (2021).
69. Grudzien-Nogalska, E. & Kiledjian, M. New insights into decapping enzymes and selective mRNA decay. *Wiley Interdisciplinary Rev. RNA* **8** https://doi.org/10.1002/wrna.1379 (2017).
70. Song, M. G., Bail, S. & Kiledjian, M. Multiple Nudix family proteins possess mRNA decapping activity. *RNA* **19**, 390–399 (2013).
71. Yan, B., Tzertzinis, G., Schildkraut, I. & Ettwiller, L. Comprehensive determination of transcription start sites derived from all RNA polymerases using ReCappable-seq. *Genome Res.* **32**, 162–174 (2022).
72. Huang, H. Y. & Hopper, A. K. Multiple layers of stress-induced regulation in tRNA biology. *Life (Basel)* **6** https://doi.org/10.3390/life6020016(2016).
73. Maraia, R. J. & Lamichhane, T. N. 3′ processing of eukaryotic precursor tRNAs. *Wiley Interdiscip. Rev. RNA* **2**, 362–375 (2011).
74. Hayashi, S., Matsui, M., Ikeda, A. & Yoshihisa, T. Six identical tRNATrpCCA genes express a similar amount of mature tRNATrpCCA but unequally contribute to yeast cell growth. *Biosci. Biotechnol. Biochem.* **86**, 1398–1404 (2022).
75. Diamond, P. D., McGlincy, N. J. & Ingolia, N. T. Depletion of cap-binding protein eIF4E dysregulates amino acid metabolic gene expression. *Mol. cell* **84**, 2119–2134.e2115 (2024).
76. Kim, K. Q. et al. eIF4F complex dynamics are important for the activation of the integrated stress response. *Mol. cell* **84**, 2135–2151.e2137 (2024).
77. Thoreen, C. C. et al. A unifying model for mTORC1-mediated regulation of mRNA translation. *Nature* **485**, 109–113 (2012).
78. Hsieh, A. C. et al. The translational landscape of mTOR signalling steers cancer initiation and metastasis. *Nature* **485**, 55–61 (2012).
79. Castelli, L. M. et al. The 4E-BP Caf20p mediates both eIF4E-dependent and independent repression of translation. *PLoS Genet.* **11**, e1005233 (2015).
80. Teleman, A. A., Chen, Y. W. & Cohen, S. M. 4E-BP functions as a metabolic brake used under stress conditions but not during normal growth. *Genes Dev.* **19**, 1844–1848 (2005).
81. Desroches Altamirano, C. et al. eIF4F is a thermo-sensing regulatory node in the translational heat shock response. *Mol. Cell* https://doi.org/10.1016/j.molcel.2024.02.038(2024).
82. Leppek, K., Das, R. & Barna, M. Functional 5′ UTR mRNA structures in eukaryotic translation regulation and how to find them. *Nat. Rev. Mol. Cell Biol.* **19**, 158–174 (2018).
83. Dvir, S. et al. Deciphering the rules by which 5′-UTR sequences affect protein expression in yeast. *Proc. Natl. Acad. Sci. USA* **110**, E2792–E2801 (2013).
84. Pelletier, J. & Sonenberg, N. Insertion mutagenesis to increase secondary structure within the 5′ noncoding region of a eukaryotic mRNA reduces translational efficiency. *Cell* **40**, 515–526 (1985).
85. Kozak, M. Influences of mRNA secondary structure on initiation by eukaryotic ribosomes. *Proc. Natl. Acad. Sci. USA* **83**, 2850–2854 (1986).
86. Brito Querido, J. et al. Structure of a human 48S translational initiation complex. *Science* **369**, 1220–1227 (2020).
87. Oliveira, C. C., van den Heuvel, J. J. & McCarthy, J. E. Inhibition of translational initiation in Saccharomyces cerevisiae by secondary structure: the roles of the stability and position of stem-loops in the mRNA leader. *Mol. Microbiol* **9**, 521–532 (1993).
88. van den Heuvel, J. J., Bergkamp, R. J., Planta, R. J. & Raue, H. A. Effect of deletions in the 5′-noncoding region on the translational efficiency of phosphoglycerate kinase mRNA in yeast. *Gene* **79**, 83–95 (1989).
89. Edwards, S. R. & Wandless, T. J. Dicistronic regulation of fluorescent proteins in the budding yeast Saccharomyces cerevisiae. *Yeast* **27**, 229–236 (2010).
90. Shichino, Y. et al. eIF4A1 enhances LARP1-mediated translational repression during mTORC1 inhibition. *Nat. Struct. Mol. Biol.* https://doi.org/10.1038/s41594-024-01321-7 (2024).
91. Rubio, C. A. et al. Transcriptome-wide characterization of the eIF4A signature highlights plasticity in translation regulation. *Genome Biol.* **15**, 476 (2014).
92. Abe, T., Nagai, R., Imataka, H. & Takeuchi-Tomita, N. Reconstitution of yeast translation elongation and termination in vitro utilizing CrPV IRES-containing mRNA. *J. Biochem.* **167**, 441–450 (2020).
93. Motohashi, K. A simple and efficient seamless DNA cloning method using SLiCE from Escherichia coli laboratory strains and its application to SLiP site-directed mutagenesis. *BMC Biotechnol.* **15**, 47 (2015).
94. Collart, M. A. & Oliviero, S. Preparation of yeast RNA. *Curr. Protoc. Mol. Biol.* Chapter 13, Unit13.12 https://doi.org/10.1002/0471142727.mb1312s23(2001).
95. Miyauchi, K., Ohara, T. & Suzuki, T. Automated parallel isolation of multiple species of non-coding RNAs by the reciprocal circulating chromatography method. *Nucleic Acids Res.* **35**, e24 (2007).
96. Suzuki, T., Ikeuchi, Y., Noma, A., Suzuki, T. & Sakaguchi, Y. Mass spectrometric identification and characterization of RNA-modifying enzymes. *Methods Enzymol.* **425**, 211–229 (2007).
97. Ohira, T. et al. Reversible RNA phosphorylation stabilizes tRNA for cellular thermotolerance. *Nature* **605**, 372–379 (2022).
98. Gietz, R. D. & Woods, R. A. Yeast transformation by the LiAc/SS Carrier DNA/PEG method. *Methods Mol. Biol.* **313**, 107–120 (2006).
99. Crooks, G. E., Hon, G., Chandonia, J. M. & Brenner, S. E. WebLogo: a sequence logo generator. *Genome Res* **14**, 1188–1190 (2004).

Acknowledgements

We thank members of the Suzuki laboratory for their continuous technical assistance and fruitful discussions, in particular Kenjyo Miyauchi for many insightful suggestions and discussions, and Haruka Shioya for providing materials. We also thank Yoshikazu Ohya (University of Tokyo), Shintaro Iwasaki (RIKEN), and Yuichi Shichino (RIKEN) for providing plasmids. We thank Junpei Morimoto (University of Tokyo), Yoshiho Ikeuchi (University of Tokyo), Yohei Kirino (Thomas Jefferson University), and Tohru Yoshihisa (University of Hyogo) for valuable discussions and critical comments on this work. This work was carried out with the support of the Isotope Science Center, University of Tokyo. Computations were partially performed on the NIG supercomputer at the ROIS National Institute of Genetics.

Author contributions

I.K. performed most of the experiments. I.K and Y.I. conducted next-generation sequencing data analyses. I.K. and T.N. performed IP-northern blotting. I.K. and T.O. performed LC/MS analyses. All authors discussed the results and revised the manuscript. I.K., Y.I., T.O., and T.S. designed the studies and wrote the manuscript. T.S. supervised the project.

Funding

This work was supported by Grants-in-Aid for Scientific Research on Priority Areas from the Ministry of Education, Science, Sports, and Culture of Japan; JSPS (26113003, 26220205, 18H05272 and 26K21763 to T.S.; 26840005 and 17H04997 to T.O.; 21J10419 to I.K.); A grant for Basic Science Research Projects to T.O. from The Sumitomo Foundation; A Kishimoto Foundation Research Grant to T.O. from Senri Life Science Foundation; A grant for young Japanese researchers to T.O. from The Nakajima Foundation; and Fusion Oriented Research for disruptive Science and Technology (FOREST; JPMJFR230S to T.O.) and Exploratory

Research for Advanced Technology (ERATO; JPMJER2002 to T.S.) from JST.

Competing interests
The authors declare no competing interests.

Additional information
Supplementary information The online version contains supplementary material available at https://doi.org/10.1038/s41467-026-76325-6.

Correspondence and requests for materials should be addressed to Takayuki Ohira or Tsutomu Suzuki.

Peer review information *Nature Communications* thanks Mark Helm, and the other, anonymous, reviewer(s) for their contribution to the peer review of this work. A peer review file is available.